NASA TECHNICAL NOTE

NASA TN D-2656

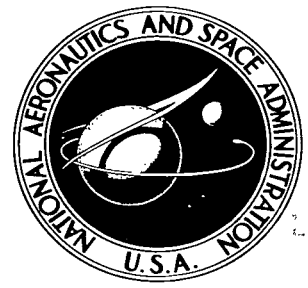

LOAN COPY: RE
AFWL (WL
KIRTLAND AFB

TECH LIBRARY KAFB, NM
0154659

NASA TN D-2656

SPIN-ENTRY CHARACTERISTICS OF A DELTA-WING AIRPLANE AS DETERMINED BY A DYNAMIC MODEL

by James S. Bowman

Langley Research Center
Langley Station, Hampton, Va.

NATIONAL AERONAUTICS AND SPACE ADMINISTRATION • WASHINGTON, D. C. • MARCH 1965

TECH LIBRARY KAFB, NM
0154659

SPIN-ENTRY CHARACTERISTICS OF A DELTA-WING AIRPLANE AS DETERMINED BY A DYNAMIC MODEL

By James S. Bowman

Langley Research Center
Langley Station, Hampton, Va.

NATIONAL AERONAUTICS AND SPACE ADMINISTRATION

For sale by the Office of Technical Services, Department of Commerce,
Washington, D.C. 20230 -- Price $2.00

SPIN-ENTRY CHARACTERISTICS OF A DELTA-WING AIRPLANE

AS DETERMINED BY A DYNAMIC MODEL

By James S. Bowman
Langley Research Center

SUMMARY

An investigation has been conducted by means of catapult tests on a 1/40-scale dynamic model to determine the spin-entry characteristics of a delta-wing airplane loaded primarily along the fuselage.

Spin-entry motions were readily obtainable for the normal center-of-gravity range of the airplane, but the motion occurred much faster for forward center-of-gravity positions than for rearward center-of-gravity positions. The use of ailerons was effective in promoting or preventing the spin entry and their effect was qualitatively the same as it was for the fully developed spin. That is, ailerons moved against the direction of yawing rotation (left when turning to right) promoted the spin entry and the use of ailerons with the direction of yawing promoted recovery from the spin entry. The optimum control technique for terminating the spin-entry motion was immediate movement of the ailerons to with the rotation, and of rudder against the rotation, while maintaining the up-elevator deflection that had caused the stall. As rotation stops, the controls should be neutralized and the stick eased forward to initiate a dive to regain flying speed.

INTRODUCTION

Spin and spin-entry investigations on bomber aircraft have not normally been conducted in the past because of maneuvering limitations usually imposed on such aircraft in the design-flight envelope. Recent design trends, however, have put some bomber aircraft in such a category as to require more maneuverability within the design-flight envelope. Subsequently, several inadvertent spin incidents have been reported, some of which involved the loss of lives and property. In an effort to permit early recognition of dangerous attitudes and motions associated with spin entry and thereby help to prevent future spin incidents, an investigation was undertaken by the NASA Langley Research Center to determine, by use of a dynamic model, the spin-entry characteristics of a delta-wing-multiengine aircraft.

The results presented in this report were obtained from tests on a dynamic model launched by a catapult. The tests were conducted at a catapult launch

facility located in a large airship hangar at the Weeksville Naval Air Facility, Elizabeth City, N.C. Radio controls were used to provide control inputs at various phases of the flight.

The spin-entry characteristics were determined for a range of center-of-gravity positions (0.275 to 0.345 percent mean aerodynamic chord) and for various control manipulations.

The angle of attack, angle of sideslip, Euler angles, and velocities of the incipient spin motions were computed from information obtained from camera measurements and the derivation of the equations used to determine these parameters is given in appendix A. The aerodynamic characteristics of the model used in the investigation are given in appendix B.

SYMBOLS

Force and moment coefficients are referred to the body-axis system except the lift and drag coefficients which are referred to the stability-axis system. Positive directions of forces, moments, and velocities are indicated in figure 1.

b	wing span, ft
C	projection of line from point at y on plate vertical center line to lens optical center on horizontal plane, in.
C_D	drag coefficient, $\frac{F_D}{\frac{1}{2}\rho V_R^2 S}$
C_L	lift coefficient, $\frac{F_L}{\frac{1}{2}\rho V_R^2 S}$
C_l	rolling-moment coefficient, $\frac{M_X}{\frac{1}{2}\rho V_R^2 Sb}$
C_m	pitching-moment coefficient, $\frac{M_Y}{\frac{1}{2}\rho V_R^2 S\bar{c}}$
C_n	yawing-moment coefficient, $\frac{M_Z}{\frac{1}{2}\rho V_R^2 Sb}$

C_Y side-force coefficient, $\frac{F_Y}{\frac{1}{2}\rho V_R^2 S}$

$C_{n_\beta} = \frac{\partial C_n}{\partial \beta}$, per deg

$C_{l_\beta} = \frac{\partial C_l}{\partial \beta}$, per deg

$C_{Y_\beta} = \frac{\partial C_Y}{\partial \beta}$, per deg

$\bar{c}$ mean aerodynamic chord, ft

d simulated horizontal distance of full-scale airplane along X" axis from origin of flight, ft

F focal length of ballistic camera lens, in.

F_D drag, lb

F_L lift, lb

F_Y side force, lb

h_A, h_B height of ballistic cameras above X'-Y' plane, ft

h_o simulated altitude of origin of flight, ft

h_Z simulated altitude of full-scale airplane on flight path, ft

I_X, I_Y, I_Z moments of inertia about X, Y, and Z body axes, respectively, slug-ft^2

$\frac{I_X - I_Y}{mb^2}$ inertia yawing-moment parameter

$\frac{I_Y - I_Z}{mb^2}$ inertia rolling-moment parameter

$\frac{I_Z - I_X}{mb^2}$ inertia pitching-moment parameter

M_X rolling moment, ft-lb

M_Y pitching moment, ft-lb

M_Z	yawing moment, ft-lb
m	mass of airplane, slugs
N	vertical distance from P to horizontal plane of lens optical centers, in.
P	position of model image nose, tail, or wing tip on ballistic camera plate
p	rolling angular velocity, deg/sec
q	pitching angular velocity, deg/sec
r	yawing angular velocity, deg/sec
R	projection of line from reference point on model to optical center of camera B lens on horizontal plane, ft
r_A, r_B	projection of line from P to lens optical center on horizontal plane, in.
S	wing area, sq ft
s	fuselage station, in.
Δt	interval between successive ballistic camera exposures, sec
u,v,w	components of velocity V_R along X, Y, and Z body axes, respectively, fps
V_R	resultant velocity, fps
$V_X", V_Y", V_Z"$	components of velocity along X", Y", Z" axes, respectively, fps
X,Y,Z	body axes
X_e, Y_e, Z_e	Euler axes
X_s, Y_s, Z_s	stability axes
X',Y',Z'	camera axes
X",Y",Z"	catapult axes
$\bar{x}$	distance of center of gravity rearward of leading edge of mean aerodynamic chord, ft
X",Z"	X"-Z" plane of the catapult-axis system

Y'',Z'' — Y"-Z" plane of the catapult-axis system

x_A,x_B — distance from P to vertical center line of camera plate (positive to right of center line), in.

y_A,y_B — distance from P to horizontal center line of camera plate (positive above center line), in.

x',y',z' — coordinates of reference point on model with respect to the camera axes, ft

x'',y'',z'' — coordinates of reference point on model with respect to catapult axes, ft

α — angle of attack, deg

β — angle of sideslip, deg

γ — flight-path angle, deg

δ — angle between camera B optical axis and X' axis

δ_a — aileron-deflection angle (negative deflection for positive rolling moment), deg

δ_e — elevator-deflection angle (negative deflection for positive pitching moment), deg

δ_r — rudder-deflection angle (negative deflection for positive yawing moment), deg

$\epsilon_A = \tan^{-1} x_A/C_A$

$\epsilon_B = \tan^{-1} x_B/C_B$

ζ — angle between line intersecting camera optical center and P on the model and the horizontal (positive when angle is above the horizontal), deg

η — ratio of distance from nose to center of gravity to fuselage length

θ_e — total angular displacement of X body axis from horizontal plane measured in vertical plane, positive when airplane nose is above horizontal plane, deg

λ — model scale factor

μ — relative density of airplane, $m/\rho Sb$

ν	angle between Y' axis and projection of optical axis of ballistic camera in horizontal plane, deg
ρ	air density, slugs/cu ft
σ_A, σ_B	angle between r_A or r_B and base line, deg
τ	vertical angle of F, positive above horizontal, deg
ϕ	angle between Y body axis and horizontal, measured in vertical plane (positive when right wing down), deg
ϕ_e	total angular displacement of Y body axis from horizontal plane measured in Y-Z body plane, positive when clockwise as viewed from rear of airplane (if X body axis is vertical, ϕ_e is measured from a reference position in horizontal plane), deg
ψ_e	horizontal component of total angular displacement of X-body axis from reference position in horizontal plane, positive when clockwise as viewed from vertically above airplane, deg

Subscripts:

A	ballistic camera (optical axis approximately perpendicular to catapult X" axis)
B	ballistic camera (optical axis parallel to catapult X" axis)
$\bar{c}$	mean aerodynamic chord of wing
cg	center of gravity
LW	left wing
le	leading edge
N	nose
n	model image number
RW	right wing
T	tail

APPARATUS AND METHODS

Model

The model used for the investigation was constructed by the NASA Langley Research Center and was made primarily of molded plastic-impregnated fiberglass. It was considered to be a 1/40-scale model of a delta-wing four-engine bomber and had a large jettisonable external store attached to the fuselage in the plane of symmetry. The dimensional characteristics of the airplane are presented in table I. A three-view drawing of the model with the external store is shown in figure 2 and a photograph is presented in figure 3.

The model was ballasted to obtain dynamic similarity to the airplane at an altitude of approximately 38,000 feet. The mass characteristics and the loading conditions investigated are presented in table II. No provision was made on the model to simulate engine thrust or gyroscopic effects of the engine.

Longitudinal and lateral control of the airplane (and model) is obtained from deflections of one set of control surfaces called elevons. Hereinafter, elevon deflections for longitudinal and lateral control are referred to, for simplicity, as elevator deflection and aileron deflection, respectively.

The maximum control deflections used on the model during the tests (measured perpendicular to the hinge lines) were:

Rudder, deg	30 right, 30 left
Elevator, deg	30 up, 5 down
Ailerons, deg	16 up, 16 down

Movement of the lateral controls of the model in flight was provided through a radio transmitter which actuated a receiver in the model. The receiver actuated an escapement mechanism which operated the model ailerons. The escapement system provided alternate neutral or preset deflections of the controls in either direction. Sufficient torque was applied to the controls to move them fully and rapidly.

Photographic Equipment

The model flights were tracked and photographed by a system of cameras to provide film coverage. Maximum contrast for photographing was obtained by darkening the building during tests and tracking the model with an arc spotlight. A perspective view of the test area, showing the arrangement of the cameras and arc light, is shown in figure 4. A projection of the cameras and catapult axes on the horizontal plane is shown in figure 5. The cameras used in the investigation included two ballistic cameras to track the model and three motion-picture cameras to pan the model for each flight. The two ballistic cameras used were set up and operated by personnel of Aeronautical Systems Division, Wright-Patterson Air Force Base, Ohio. These cameras were rigidly mounted on towers at an elevation of 50 feet, and recorded images of the model throughout each flight were obtained at the rate of 18 exposures per second on a 12.5-inch-square

glass plate. The shutters on each camera were electrically synchronized with each other to an accuracy of 2 milliseconds. The lens focal lengths (253 mm) were measured at the test site to an accuracy of 0.01 millimeter. Each lens had a 60° conical field of view. The ballistic cameras were arranged so that the optical axis of one camera (camera A) was approximately perpendicular to the X" axis of the catapult, and the optical axis of the other camera (camera B) was parallel to the X" axis of the catapult and in the horizontal plane. The optical axis of camera A was inclined upward 7.5° with respect to the horizon and turned 7.5° toward the catapult (fig. 5). Reference points were established on the glass plates of the ballistic camera by a set of reference lights (figs. 4 and 5).

Testing Technique

The catapult was located at an elevation of 137 feet above the ground and was adjustable so that the model flight path γ, the angle of pitch θ_e, and the launch velocity could be varied for each launch condition. A sketch of the relationship of the catapult and the model is presented in figure 6. The model was launched with an angle of attack of 20° with the elevator deflection set for trim flight. The model was generally launched with the elevators held in the trim condition by a pin, but preloaded to move to a preset deflection that would induce a stall. After the launch, the pin was pulled by a light string (or static line) to allow the elevator to move and stall the model. The ailerons were deflected by a radio signal at any time desired during the flight. Each flight was terminated as the model landed in a large net near the ground. The model was then retrieved for another launch. The data obtained in this investigation include a complete time history of the angle of attack, angle of sideslip, flight-path angle, attitude angles, and linear and angular velocities for each flight. The data were reduced by the method described in appendix A.

Accuracy

The weight and mass characteristics of the model given in table II are believed to be accurate within the following limits:

Weight, percent	±1
Center of gravity, percent $\bar{c}$	±0.05
Moments of inertia, percent	±5

The accuracy of obtaining measurements from the glass-plate negatives for data reduction is illustrated by a sample run presented in figure 7. Measurements were taken from the glass plate of this run at two different times and the results from the two sets of readings are plotted for comparison.

RESULTS AND DISCUSSION

Time histories showing typical results of the investigation are presented in figures 8 to 15. The results obtained with the large external store indicated

that it had no noticeable effect on the spin-entry characteristics and, in addition, no effect of gross weight could be seen. All the results presented in this investigation, therefore, represent typical results that were obtained with the store on or off and for the gross-weight range investigated.

The model used in this investigation usually entered a spinning motion to the left. It has been shown in force tests (refs. 1 and 2) that pointed-nose designs can have large asymmetrical yawing moments at high angles of attack. This asymmetry is due to a random separation of the vortex off the sharp pointed nose. In the case of the model of the present investigation, the yawing moment was consistently to the left apparently because of some small geometric asymmetry in the forward fuselage section that triggered the vortex separation and caused the left entry. Spin-tunnel tests of the developed spin have shown similar results (ref. 1), in that the moments resulting from such asymmetric separation can cause a model to spin readily in one direction and not in the other direction, and that by rotating a small portion of the nose through a given angle, the direction in which the model readily spins can be reversed. Unpublished flight-test information indicates that airplanes apparently experience this same phenomena because several sharp-nosed designs have shown a greater tendency to spin in one direction than the other. Force-test data available for a model of the same design and scale as that used in this investigation show that large yawing-moment and side-force asymmetries would be expected to occur on this design in the angle-of-attack range from about 40° to 60° (fig. 16). These data show an asymmetry to the right, but the model used in the present investigation apparently had a similar asymmetry to the left.

The post-stall characteristics of the model with rudder and aileron deflections of zero and for the center-of-gravity range investigated are presented in figures 8 to 11. These data show that spin-entry motions were readily obtained at the forward center-of-gravity position of $0.275\bar{c}$ (fig. 8). The entry was a smooth and coordinated maneuver and was characterized by a dropping of the nose with simultaneous rolling and yawing to the left (for left entry). As the center of gravity was moved rearward, the spin-entry motion developed more slowly (figs. 9 and 10 for center-of-gravity locations of $0.295\bar{c}$ and $0.315\bar{c}$, respectively) and, at the most rearward center-of-gravity position ($0.345\bar{c}$, fig. 11), no appreciable yawing motion developed. This characteristic can be seen in the rate of change of the ψ_e curve. The motion in which no appreciable yaw developed was characterized by large pitch oscillations with relatively little roll. This effect of center-of-gravity location on the post-stall and spin-entry characteristics is shown in the summary plot in figure 17. In this figure, the time for the model to yaw 1/2 turn in the incipient-spin motion is shown for various center-of-gravity positions and for zero rudder and aileron deflection and includes the results of many tests and not just those of figures 8 to 11. As can be seen from figure 17, the time for the first half turn increases appreciably as the center of gravity moves rearward. The aerodynamic data in figure 18 show that the model had neutral static longitudinal stability for the $0.315\bar{c}$ center-of-gravity location and, therefore, a more rearward center of gravity would not be considered to be a normal operating condition. The foregoing spin-entry results therefore indicate that the model would readily enter a spin for the normal range of center-of-gravity locations. These results are in general agreement with the spin-tunnel-test results for the developed spin for a similar model which shows that the model was much more prone to spin for

the forward center-of-gravity position than for the rearward center-of-gravity position.

The effects of aileron deflection on the spin-entry characteristics are shown in figures 12 to 15. The effects of pro-spin and antispin ailerons are presented in figures 12 and 13, respectively, for a center-of-gravity position of $0.275\bar{c}$ and in figures 14 and 15, respectively, for a center-of-gravity position of $0.315\bar{c}$.

As previously pointed out, the model has a strong tendency to enter a spin at the forward center-of-gravity position and, for that reason, the effects of pro-spin deflections are not readily discernible for this center-of-gravity position (fig. 12). The use of antispin aileron deflection, however, was effective in preventing the spin-entry motion (fig. 13) and the model yawed slowly to the right.

Aileron deflections had a more noticeable effect on the model motions when the center of gravity was located rearward of the $0.275\bar{c}$ position. For a center-of-gravity position of $0.315\bar{c}$ (fig. 14), pro-spin aileron deflection caused a much more rapid spin entry than was obtained with zero aileron deflections. When the ailerons were deflected pro-spin (fig. 14), the model yawed the first half turn in about 6 seconds whereas about 18 seconds were required when the aileron deflection was zero (fig. 10). When antispin aileron control was used (fig. 15), a recovery from the entry into a left spin was effected; and it appears from the time history that the model started into a right spin which might be expected since the initial corrective-control deflection was maintained.

The foregoing effect of aileron deflection on the spin entry correlates well with the effect of ailerons on fully developed spins. As pointed out in previous studies such as reference 1, the aileron effect is highly dependent upon the loading characteristic of the airplane. In general, when the mass is located primarily along the fuselage, aileron-with the spin and elevator-up settings aid spin recoveries. The model used in this investigation was loaded primarily along the fuselage (table II), and the aileron effect found for spin entry is in agreement with the foregoing generalization and with the aileron effect found for developed spins for the same configuration.

From the results of this investigation, it is apparent that the deflection of the ailerons could be very important during inadvertent post-stall and incipient-spin motions, particularly for airplanes loaded primarily along the fuselage. Extreme care should be taken not to try to lift the wing with ailerons when flying near, or just beyond the stall; and, in addition, the ailerons should not be allowed to deflect against the direction of yaw during attempted recoveries from incipient spin. Recoveries from post-stall and incipient-spin motions by moving the stick forward (elevators down) could be effective provided this action is taken soon enough after the stall, but if initiated too late, stick forward could be adverse and probably cause the rate of rotation to increase rather than cause the airplane to nose down.

Based on the present tests and past experience with full-scale and model spin characteristics, the recommended recovery technique for incipient spins for airplanes loaded primarily along the fuselage, therefore, is movement of the

ailerons immediately to full with the direction of yawing (stick right for rotation to the right) and movement of the rudder to oppose the yawing, even though the rudder may not be very effective, while maintaining the up-elevator deflection that had caused the stall. As rotation stops, the controls should be neutralized and the stick eased forward to regain flying speed. Because of the very limited experience with recoveries from incipient spins, however, the actual sequence for the best recovery for a specific design should be confirmed by full-scale flight tests. Recoveries attempted during the incipient phase of the spin would be expected to be more rapid than those from the fully developed spin because of the fact that rotation rate is lower in the incipient-spin phase than for the fully developed spin.

CONCLUDING REMARKS

An investigation has been conducted by catapulting a dynamically scaled model into free flight to determine the incipient-spin and recovery characteristics of a delta-wing airplane configuration loaded primarily along the fuselage. The following conclusions are made based on the results of the investigation:

1. The incipient-spin motion was readily obtainable for the normal center-of-gravity range of the design.

2. Center-of-gravity location had a pronounced effect on the spin entry characteristics. The entry motion occurred faster for forward center-of-gravity positions than for rearward center-of-gravity positions.

3. The use of ailerons was very effective in promoting or preventing the incipient spin and the direction that they should be moved for recovery was found to be the same as that for recovery from the fully developed spin.

4. For airplanes loaded primarily along the fuselage, the following technique is recommended for recovery from incipient spins: move the ailerons immediately to full with the direction of yaw (stick right for rotation to the right) and move the rudder against the direction of yaw with the elevator maintained at the up deflection that had caused the stall. As rotation stops, the controls should be neutralized and the stick eased forward to regain flying speed.

Langley Research Center,
National Aeronautics and Space Administration,
Langley Station, Hampton, Va., August 10, 1964.

APPENDIX A

DERIVATION OF EQUATIONS FOR EVALUATION OF PARAMETERS IN INCIPIENT-SPIN MOTION

The angle of attack, angle of sideslip, Euler angles, and the velocities of the model in flight are based on the location and attitude of the model in space with respect to the earth axis. The determination of the velocities is accomplished by differentiating the respective earth-axis space coordinates of the model with respect to time to obtain the earth-axis velocities of the model and then, by resolving by trigonometric means, the velocities about a body-axis system are computed. The velocities about the body axis are used to determine angle of attack and angle of sideslip.

The axis systems used for determining the space coordinates of reference points on the model (nose, tail, and wing tips) are illustrated in figure 5. The camera axis system (X', Y', Z') has its origin at a point at the test-area floor level directly beneath the optical center of the lens of camera B. The Y' axis extends horizontally through a point directly beneath the optical center of the lens of camera A. The X' axis is oriented horizontally through the origin at right angles to the Y' axis. The Z' axis passes vertically through the origin, with upward values considered positive. The origin of the catapult axis system (X", Y", Z") is approximately at the release point of the catapult. The X" and Y" axes are horizontal, and parallel and perpendicular to the launching-track center line, respectively. The Z" axis passes vertically through the origin and is considered positive downward.

Figure 20 shows the initial projection of the reference points on the model to the horizontal plane of the optical centers of the camera lens. (The camera plates in the sketch are shown "reflected" at the focal length distance in front of the lenses.) The coordinates (x_A, y_A, x_B, y_B) of a point P on each plate (denoting a specific point on the model for corresponding images) are determined with respect to the horizontal and vertical center lines of the plate. The point is projected to the optical center of the lens plane and the horizontal angles are determined for each camera with respect to the "base line" (a line parallel to the Y' axis through the lens optical centers) as follows:

$$\left.\begin{aligned} C_A &= F_A \cos \tau_A - y_A \sin \tau_A \\ N_A &= F_A \sin \tau_A + y_A \cos \tau_A \\ \epsilon_A &= \tan^{-1} \frac{x_A}{C_A} \\ \sigma_A &= \nu_A + \epsilon_A \end{aligned}\right\} \text{For left wing, right wing, nose, and tail from plates of cameras A and B}$$

The same equations with appropriate subscripts apply to camera B.

The vertical angle of the point at camera B with respect to the optical center of the lens plane is determined as follows:

$$\left.\begin{aligned} r_B &= \frac{C_B}{\cos \epsilon_B} \\ \tan \zeta_B &= \frac{N_B}{r_B} \end{aligned}\right\} \quad \text{For left wing, right wing, nose, and tail from plate of camera B only}$$

The expression:

$$R = \frac{\text{Length of base line}\left(\sin \sigma_A\right)}{\sin\left(\sigma_A - \sigma_B\right)}$$

gives the distance to the projection of the point on the model in the horizontal plane.

The coordinates of the point with respect to the camera axis system (X', Y', Z') are then:

$$x' = R \sin \sigma_B$$

$$y' = R \cos \sigma_B$$

$$z' = h_B + R \tan \zeta_B$$

In transferring from the camera axis system to the catapult axis system the axes are translated and rotated so that the positive direction of Z" is oriented downward. The distances from the camera-axis origin to the catapult-axis origin along the catapult axes are 227.5 feet on the X" axis, 5.75 feet on the Y" axis, and 137 feet on the Z" axis. The coordinates of a point with respect to the catapult axes are:

$$x'' = -(x' \cos \delta + y' \sin \delta) + 227.5$$

$$y'' = -(x' \sin \delta - y' \cos \delta) + 5.75$$

$$z'' = -z' + 137$$

By knowing the location of the model right wing, left wing, nose, and tail for each image along the flight path, the attitude of the model, and, consequently, the rate of change of attitude, can be computed.

The values of x", y", and z" with respect to the center of gravity are determined as follows:

$$s_{cg} = s_{lec} + \bar{x}$$

$$\eta = \frac{s_{cg} - s_N}{s_T - s_N}$$

$$x"_{cg} = x"_N + \left(x"_T - x"_N\right)\eta$$

$$y"_{cg} = y"_N + \left(y"_T - y"_N\right)\eta$$

$$z"_{cg} = z"_N + \left(z"_T - z"_N\right)\eta$$

By using x", y", and z" at the center of gravity of the model, the flight-path projection into the vertical plane is given as follows, with n-1, n, n+1, being the sequence of points used to determine γ at the time n.

$$\tan \gamma_{X,Z} = \frac{1}{2}\left(\frac{z"_n - z"_{n+1}}{x"_n - x"_{n+1}} + \frac{z"_{n-1} - z"_n}{x"_{n-1} - x"_n}\right)$$

$$\tan \gamma_{Y,Z} = \frac{1}{2}\left(\frac{z"_n - z"_{n+1}}{y"_n - y"_{n+1}} + \frac{z"_{n-1} - z"_n}{y"_{n-1} - y"_n}\right)$$

$$\tan \gamma = -\frac{1}{\sqrt{\frac{1}{\tan^2\gamma_{X,Z}} + \frac{1}{\tan^2\gamma_{Y,Z}}}}$$

The simulated altitude of the model is given as:

$h_z = h_o - z"\lambda$ and distance along the X" axis by: $d = x"\lambda$

The Euler space angles θ_e, ϕ_e, and ψ_e are computed as follows:

$$\cos \theta_e = \frac{\sqrt{\left(x"_N - x"_T\right)^2 + \left(y"_N - y"_T\right)^2}}{\sqrt{\left(x"_N - x"_T\right)^2 + \left(y"_N - y"_T\right)^2 + \left(z"_N - z"_T\right)^2}}$$

$$\sin \phi_e = \frac{\sin \phi}{\cos \theta_e}$$

where

$$\sin \phi = \frac{\left(z''_{RW} - z''_{LW}\right)}{\sqrt{\left(x''_{RW} - x''_{LW}\right)^2 + \left(y''_{RW} - y''_{LW}\right)^2 + \left(z''_{RW} - z''_{LW}\right)^2}}$$

and

$$\cos \psi_e = \frac{\left(x''_N - x''_T\right)}{\sqrt{\left(x''_N - x''_T\right)^2 + \left(y''_N - y''_T\right)^2}}$$

In order to determine the proper sign for θ_e and ψ_e, the following sign convention was used (θ_e was considered positive when the nose was above the horizon and negative when the nose was below the horizon):

Sign of $\left(z''_N - z''_T\right)$	Quadrant	Degrees
+	IV	0 to -90
-	I	0 to +90

(ψ_e was considered positive clockwise, and the quadrant determined as follows):

Sign of $\left(x''_N - x''_T\right)$	Sign of $\left(y''_N - y''_T\right)$	Quadrant	Degrees
+	+	I	0 to 90
-	+	II	90 to 180 (180° - angle)
-	-	III	180 to 270 (180° + angle)
+	-	IV	270 to 360 (360° - angle)

The velocity of the model along the X", Y", and Z" axes was computed as follows:

$$V_{X''} = \left(\frac{x''_{n+1} - x''_{n-1}}{2\Delta t}\right)\sqrt{\lambda}$$

$$V_{Y''} = \left(\frac{y''_{n+1} - y''_{n-1}}{2\Delta t}\right)\sqrt{\lambda}$$

$$V_{Z''} = \left(\frac{z''_{n+1} - z''_{n-1}}{2\Delta t}\right)\sqrt{\lambda}$$

The velocity along the body axes X, Y, and Z was computed as u, v, and w, as follows:

$$u = \left(V_{X''} \cos \psi_e + V_{Y''} \sin \psi_e\right)\cos \theta_e - V_{Z''} \sin \theta_e$$

$$v = \left(-V_{X''} \sin \psi_e + V_{Y''} \cos \psi_e\right)\cos \phi_e + \left[\left(V_{X''} \cos \psi_e + V_{Y''} \sin \psi_e\right)\sin \theta_e + V_{Z''} \cos \theta_e\right]\sin \phi_e$$

$$w = -\left(-V_{X''} \sin \psi_e + V_{Y''} \cos \psi_e\right)\sin \phi_e + \left[\left(V_{X''} \cos \psi_e + V_{Y''} \sin \psi_e\right)\sin \theta_e + V_{Z''} \cos \theta_e\right]\cos \phi_e$$

The angle of attack and sideslip can now be computed by:

$$\alpha = \tan^{-1} \frac{w}{u}$$

and

$$\beta = \sin^{-1} \frac{v}{V_R}$$

where

$$V_R = \sqrt{u^2 + v^2 + w^2}$$

The angular velocities p, q, and r were determined as follows:

$$\dot{\psi}_e = \frac{1}{2\Delta t}\left(\psi_{e,n+1} - \psi_{e,n-1}\right)$$

$$\dot{\theta}_e = \frac{1}{2\Delta t}\left(\theta_{e,n+1} - \theta_{e,n-1}\right)$$

$$\dot{\phi}_e = \frac{1}{2\Delta t}\left(\phi_{e,n+1} - \phi_{e,n-1}\right)$$

$$p = \left(-\dot{\psi}_e \sin \theta_e + \dot{\phi}_e\right)$$

$$q = \dot{\psi}_e \cos \theta_e \sin \phi_e + \theta_e \cos \phi_e$$

$$r = \dot{\psi}_e \cos \theta_e \phi_e - \theta_e \sin \phi_e$$

APPENDIX B

AERODYNAMIC CHARACTERISTICS OF THE MODEL

Force data presented in figures 18, 19, 21, and 22 show, in general, longitudinal and lateral stability characteristics of the design investigated. These data were obtained from reference 3. The data presented correspond to a Mach number of 0.21, and a Reynolds number of 1,190,000 based on a wing mean aerodynamic chord of 0.904 foot.

Longitudinal Stability

The longitudinal stability characteristics of the model are presented in figure 18 for a range of center-of-gravity positions. As indicated by the slope of the pitching-moment curve, the static stability is approximately neutral at $0.315\bar{c}$. Presented in figure 21 is the effect of elevator deflection on the lift and drag characteristics for an angle-of-attack range from 0° to 90°.

Lateral Stability

The lateral and directional static stability parameters are presented in figures 19 and 22 for angles of attack from 0° to 80°. The data are presented in terms of the effective-dihedral parameter C_{l_β} (fig. 22), the side-force parameter C_{Y_β} (fig. 22), and the directional-stability parameter C_{n_β} (fig. 19). These data were obtained for sideslip angles of $\pm 5^{\circ}$. The directional-stability parameter is plotted for the four different center-of-gravity locations covered in the spin entry tests, and show virtually no effect of center-of-gravity location.

REFERENCES

1. Neihouse, Anshal I., Klinar, Walter J., and Scher, Stanley H.: Status of Spin Research for Recent Airplane Designs. NASA TR R-57, 1960. (Supersedes NACA RM L57F12.)

2. Letko, William: A Low-Speed Experimental Study of the Directional Characteristics of a Sharp-Nosed Fuselage Through a Large Angle-of-Attack Range at Zero Angle of Sideslip. NACA TN 2911, 1953.

3. Ammann, Victor R., Jr.: Wind Tunnel Data Report - Low Speed Tests of the 1/40-Scale B-58A High Angle Stability Force Model. Rept. FZT-4-231 (Contract No. AF 33(600)-36200), Gen. Dyn./Ft. Worth, Jan. 18, 1961.

TABLE I.- FULL-SCALE DIMENSIONAL CHARACTERISTICS OF AIRPLANE AS TESTED ON THE 1/40-SCALE MODEL

Overall length, ft	96.78
Depth of fuselage at wing-fuselage intersection, ft	6.34
Wing:	
Area, sq ft	1542.53
Span, ft	56.828
$\bar{c}$, in.	434.049
Distance from LE wing root chord to LE $\bar{c}$, in.	196.97
Distance from fuselage center line to wing $\bar{c}$, in.	113.72
Aspect ratio	2.096
Taper ratio	0
Root chord, ft	54.256
Airfoil section:	
Root	NACA 0003.46-69.069
Outboard of full-scale span station 56.5 in.	NACA 0004.08-63
Incidence, deg	3.00
Dihedral, deg	2.229
Sweepback at LE, deg	60
Sweepback at TE, deg	-10
Elevons:	
Area, both elevons, sq ft	177.832
Span (from station 56.5 in. to station 237.0 in.), ft	15.042
Vertical stabilizer:	
Area (exposed), sq ft	160.00
Span, ft	14.50
Sweepback at LE, deg	52.00
Sweepback at TE, deg	26.707
Aspect ratio	2.628
Taper ratio	0.324
Root chord, ft	16.667
Tip chord, ft	5.402
Rudder:	
Area, sq ft	40.00
Hinge-line sweepback, deg	35.5
Nacelle location:	
Distance of inboard nacelle from fuselage center line, in.	146.00
Distance of outboard nacelle from fuselage center line, in.	260.00
Store:	
Overall length, ft	57.65
Maximum diameter, in.	60.00
Distance from nose of fuselage to nose of pod, in.	158.00
Distance from fuselage reference line to center line of pod, in.	72.960

TABLE II.- MASS CHARACTERISTICS AND INERTIA PARAMETERS FOR THE LOADINGS TESTED ON THE 1/40-SCALE DYNAMIC MODEL

[Values given are full scale and moments are about the center of gravity]

Configuration	Weight, lb	Center-of-gravity location, percent $\bar{c}$	Relative density, μ, at		Moments of inertia, slug-ft^2			Mass parameters		
			Sea level	38,000 ft	I_X	I_Y	I_Z	$\frac{I_X - I_Y}{mb^2}$	$\frac{I_Y - I_Z}{mb^2}$	$\frac{I_Z - I_X}{mb^2}$
Basic model	61,230	27.5	9.12	33.88	269,261	696,436	939,738	-681×10^{-4}	-388×10^{-4}	1069×10^{-4}
	61,230	29.5	9.12	33.88	269,261	672,753	916,055	-644×10^{-4}	-388×10^{-4}	1032×10^{-4}
	61,230	31.5	9.12	33.88	269,011	643,159	886,710	-621×10^{-4}	-404×10^{-4}	1025×10^{-4}
	61,230	34.5	9.12	33.88	269,011	546,424	789,976	-460×10^{-4}	-404×10^{-4}	864×10^{-4}
Basic model with external store	71,900	27.5	10.71	39.78	290,564	847,205	1,121,680	-767×10^{-4}	-378×10^{-4}	1145×10^{-4}
	71,900	29.5	10.71	39.78	302,244	755,013	1,021,325	-628×10^{-4}	-370×10^{-4}	998×10^{-4}
	71,900	31.5	10.71	39.78	297,992	693,412	963,963	-549×10^{-4}	-375×10^{-4}	924×10^{-4}
	71,900	34.5	10.71	39.78	298,359	677,795	947,992	-527×10^{-4}	-375×10^{-4}	902×10^{-4}
	101,450	27.5	15.11	56.14	346,265	840,572	1,146,762	-492×10^{-4}	-305×10^{-4}	797×10^{-4}
	101,450	31.5	15.11	56.14	348,645	835,648	1,139,458	-485×10^{-4}	-303×10^{-4}	788×10^{-4}
	101,450	34.5	15.11	56.14	346,265	694,623	1,000,813	-347×10^{-4}	-305×10^{-4}	652×10^{-4}

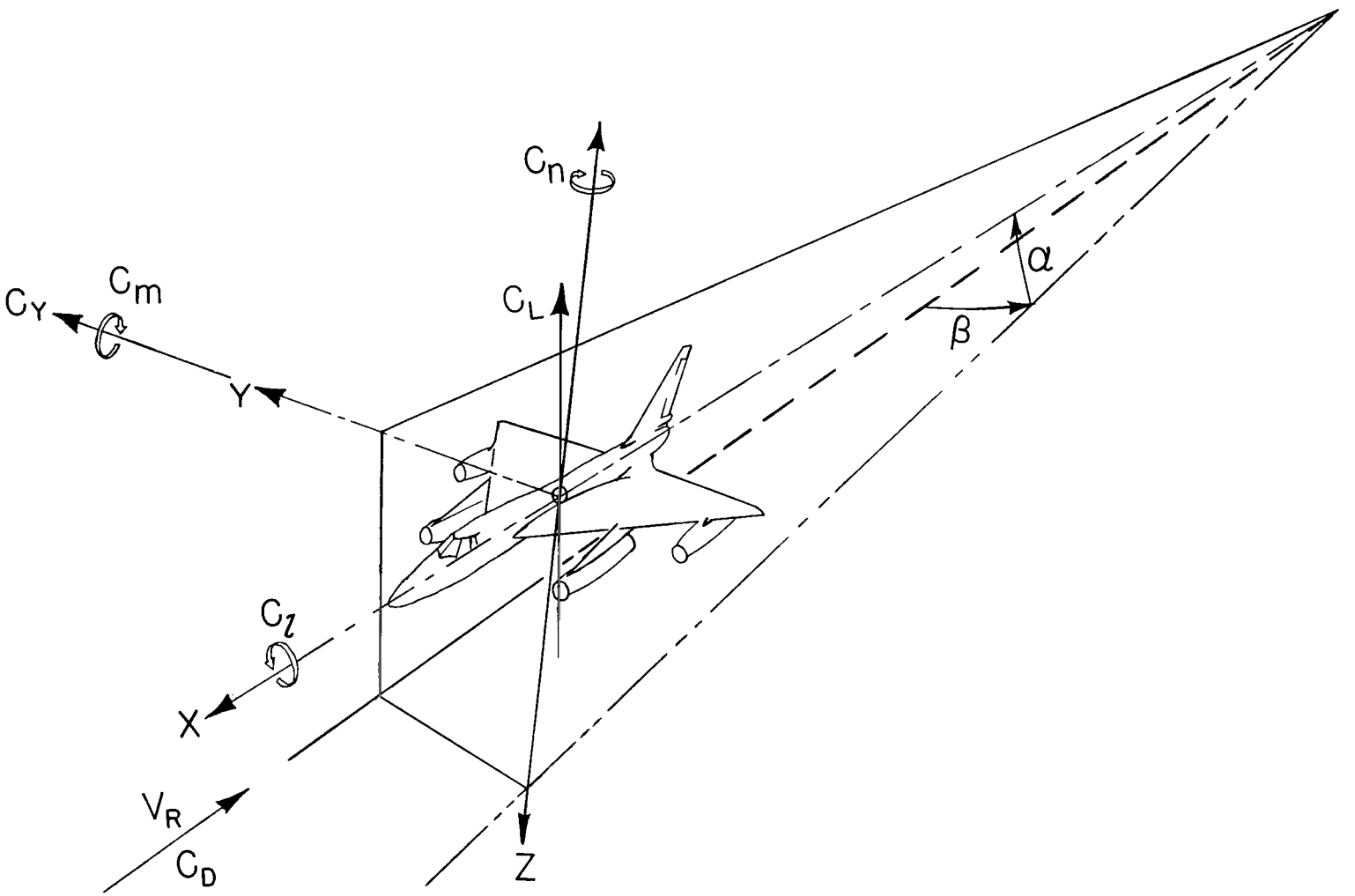

(a) Positive direction of forces and moments about body-axis system.

Figure 1.- Axis systems.

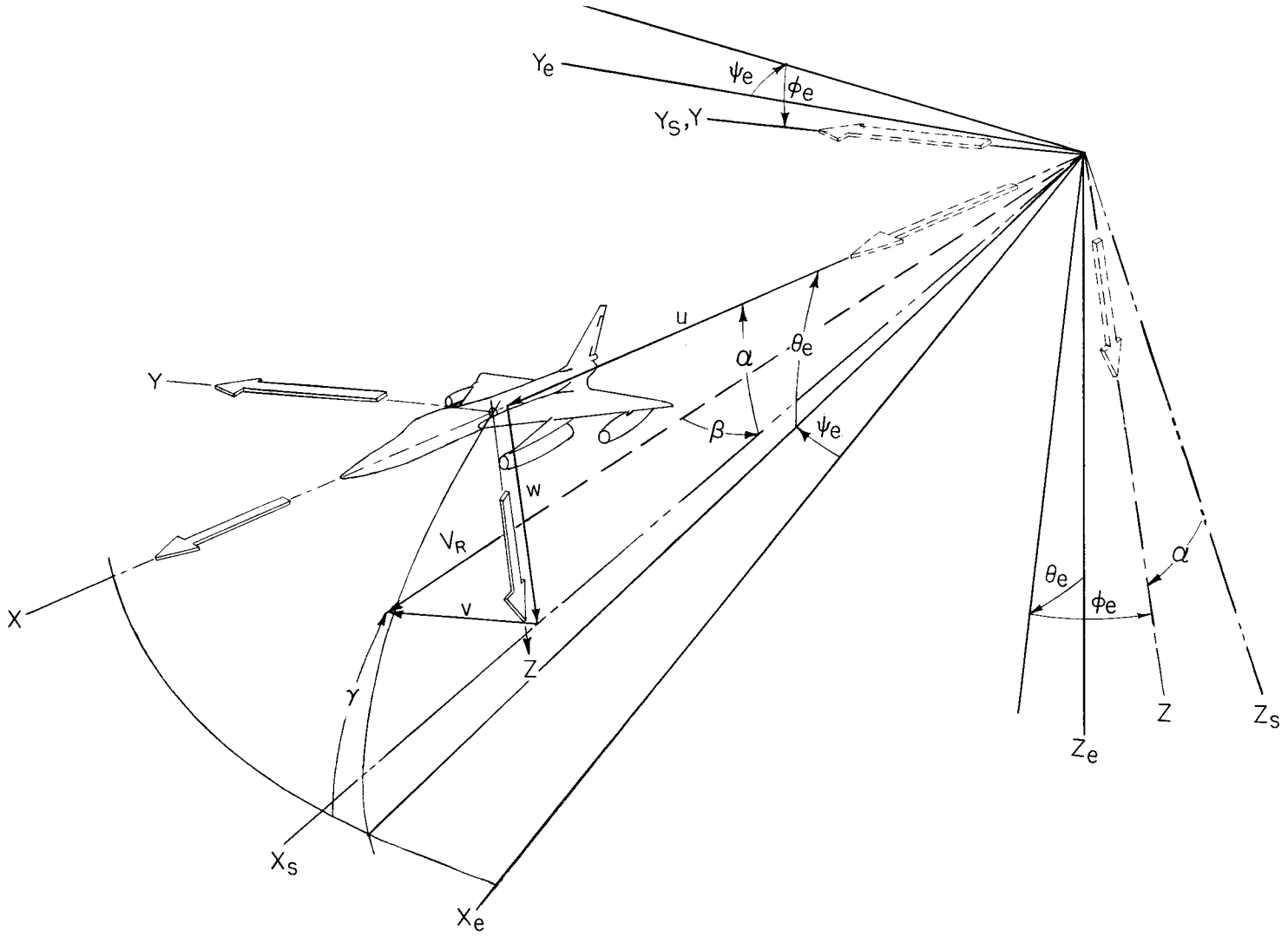

(b) Relation between body-, stability-, and Eular axis systems. Velocities and angles are shown in the positive direction.

Figure 1.- Concluded.

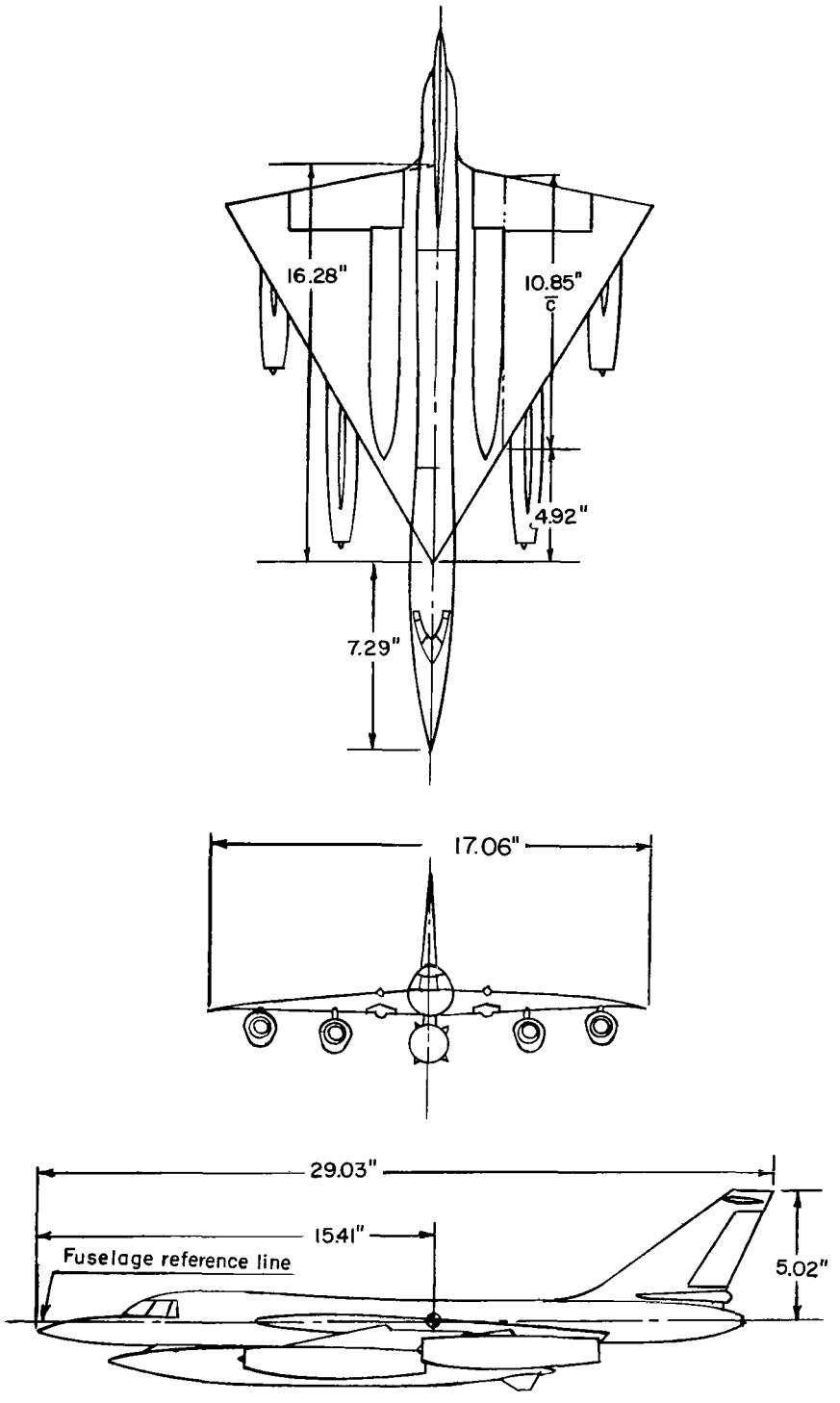

Figure 2.- Three-view drawing of the model. Basic model with store shown for center of gravity at 29.5 percent $\bar{c}$.

Figure 3.- Basic model with store. L-60-6466

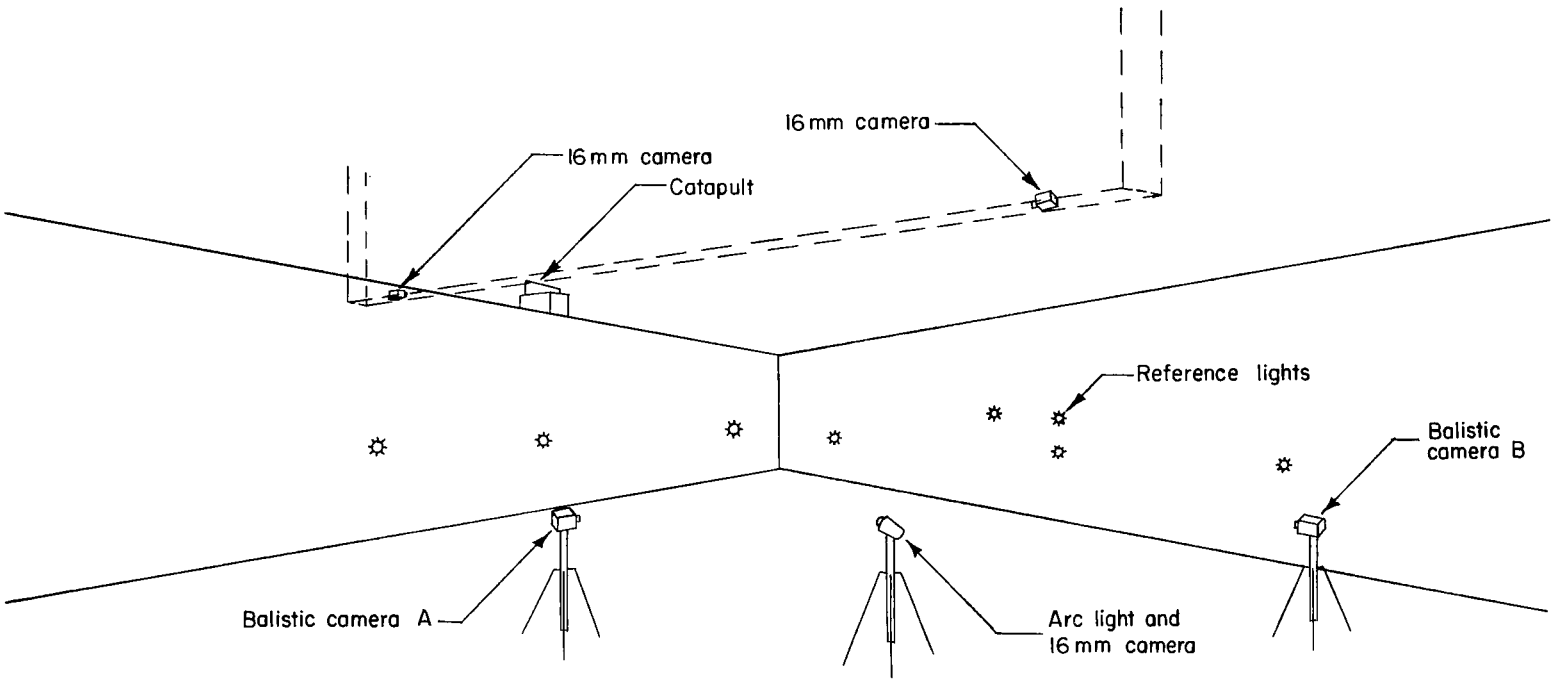

Figure 4.- Perspective view of test area showing relative locations of photographic equipment, reference lights, and catapult.

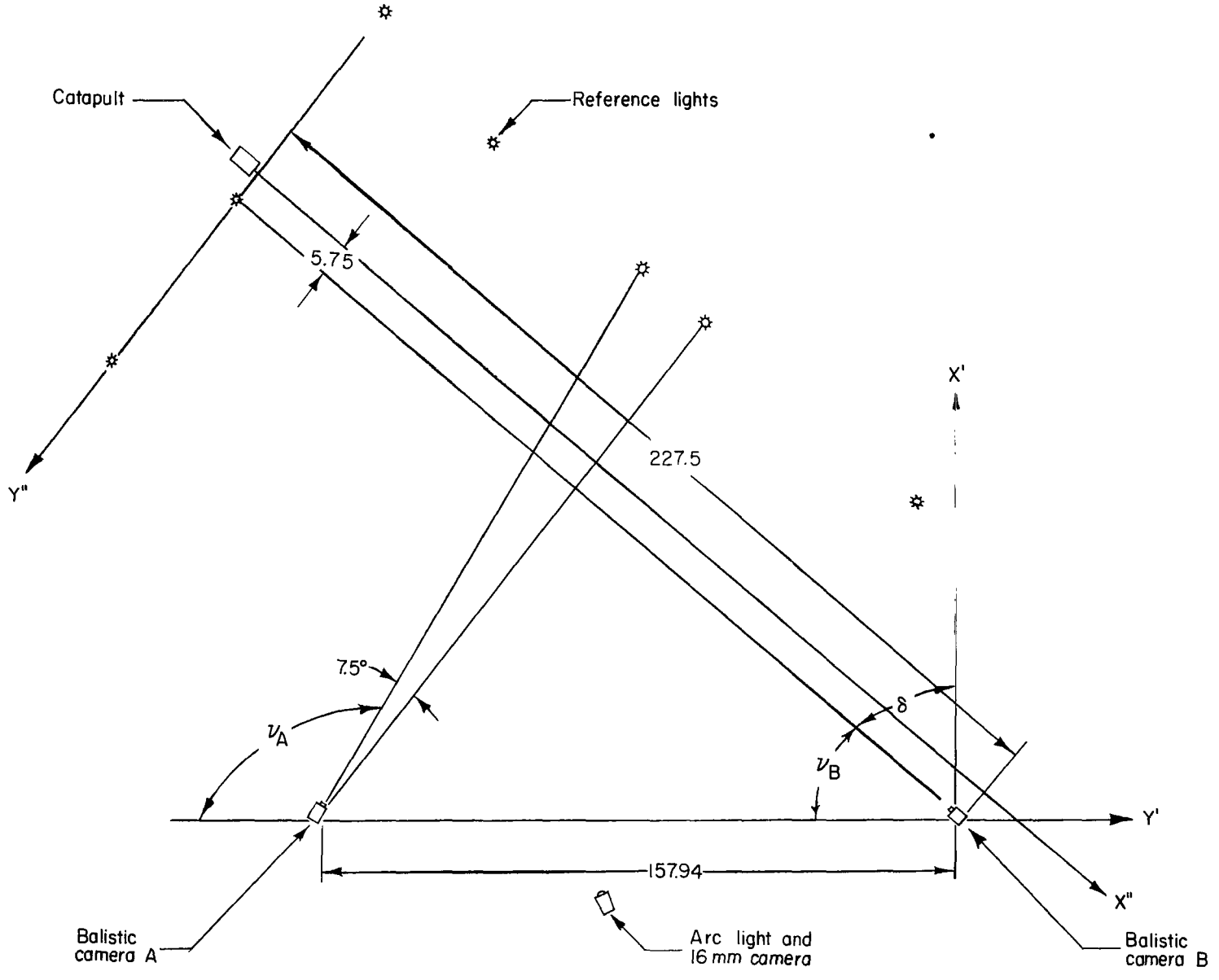

Figure 5.- Projection of camera and catapult axis on horizontal plane. Dimensions are in feet.

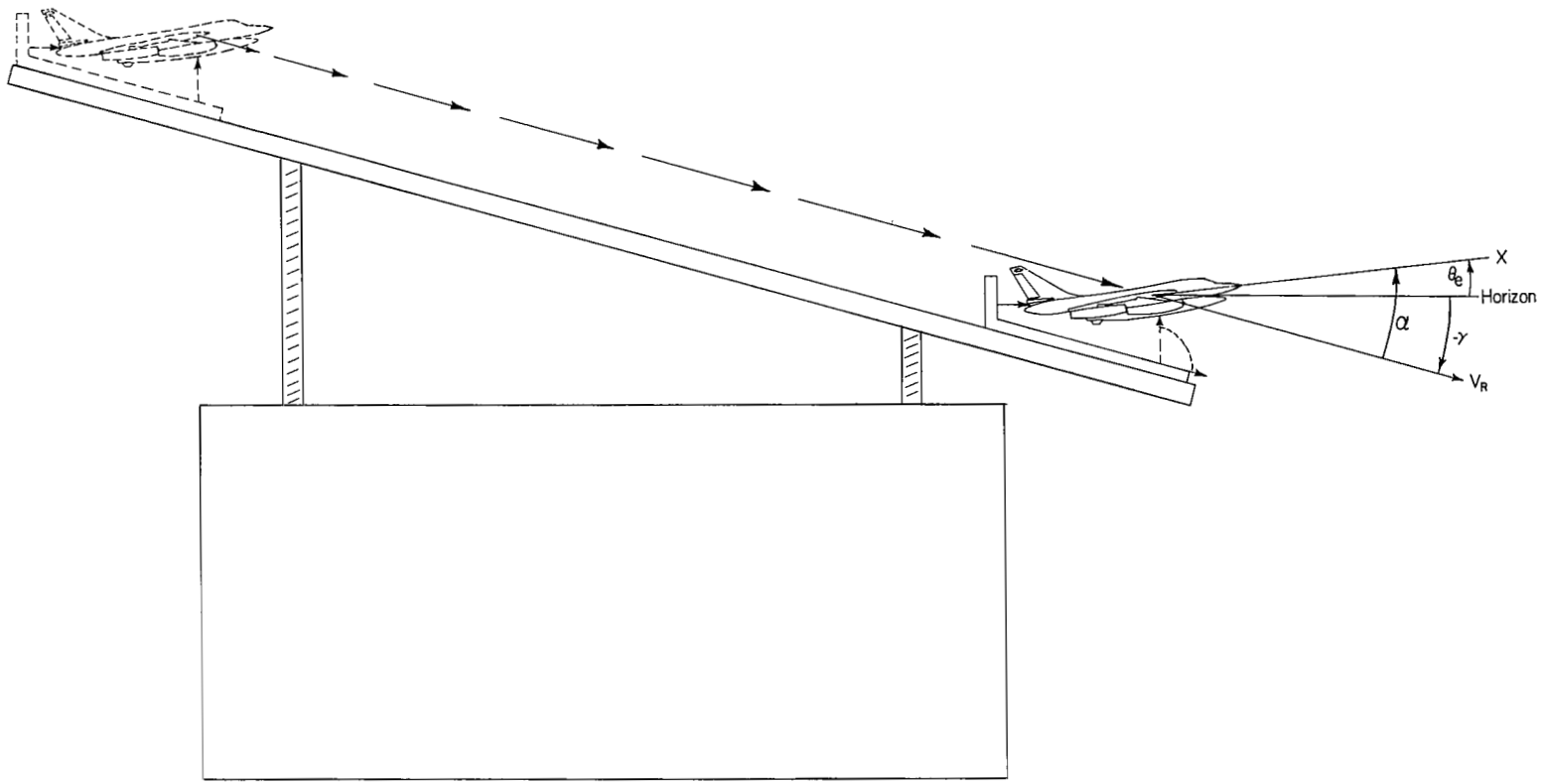

Figure 6.- Sketch showing related attitude of model and catapult at launch. Positive direction of velocity and angles are shown except γ which is negative.

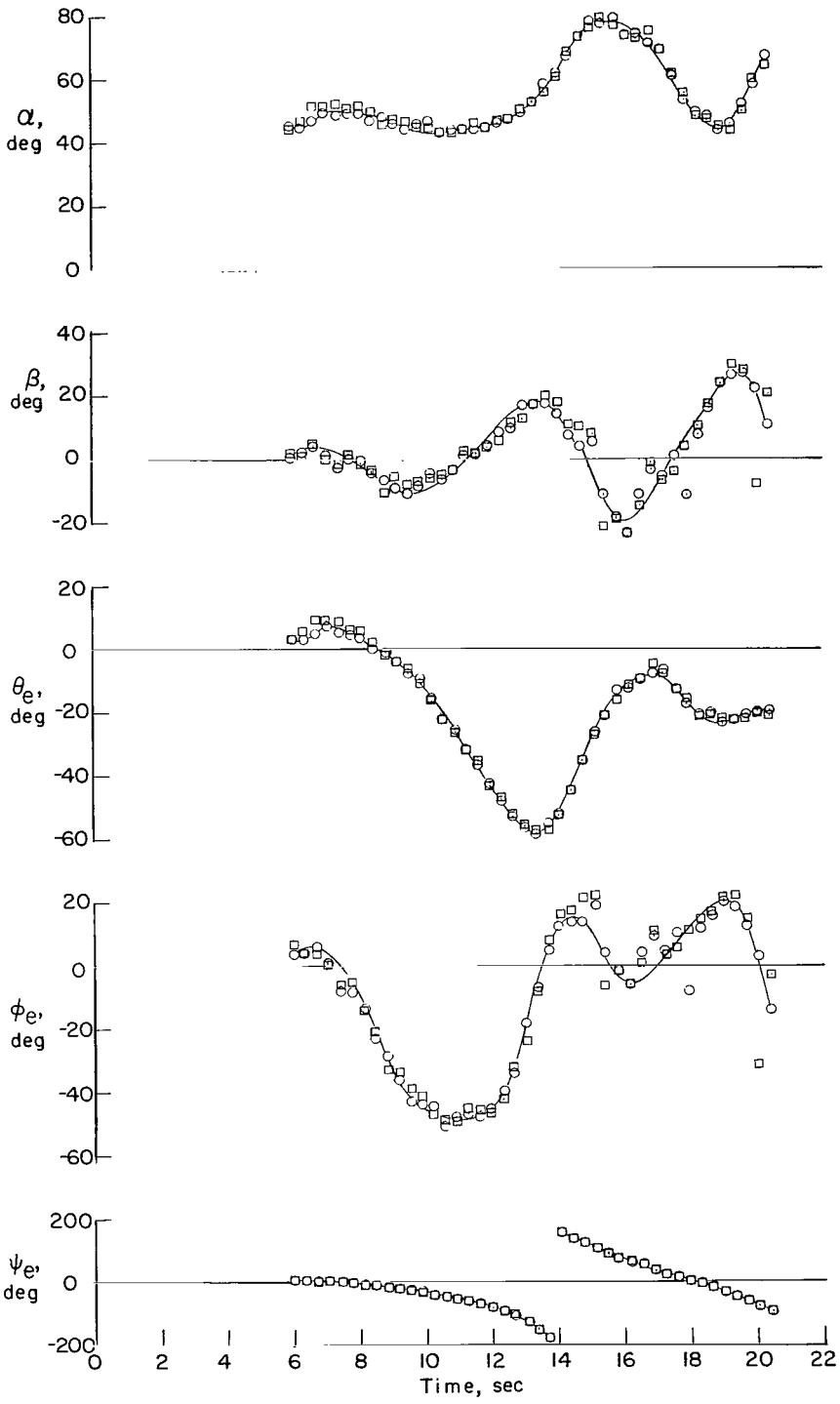

Figure 7.- Comparison of measurements taken from glass-plate negatives for two typical model flights.

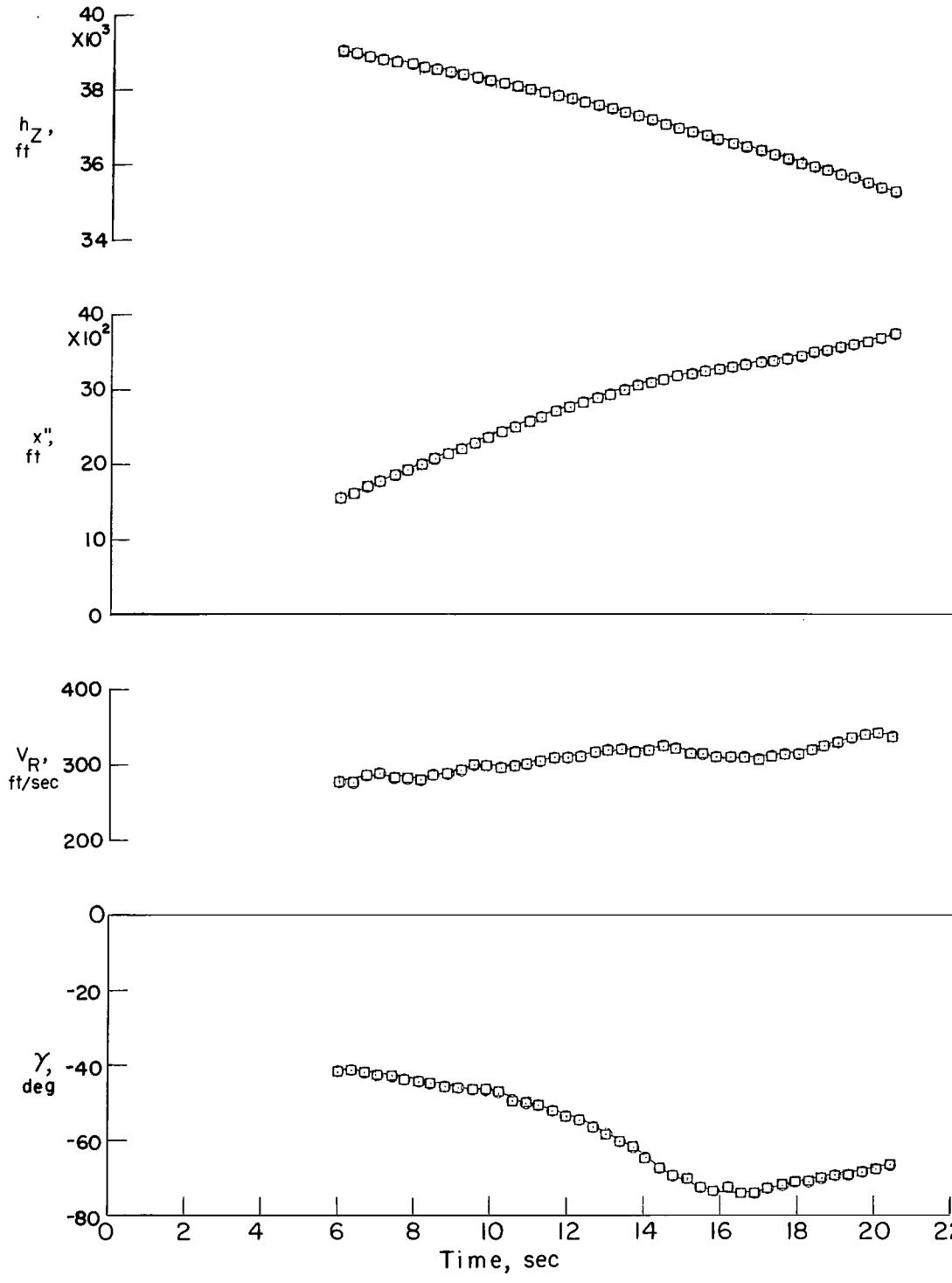

Figure 7.- Concluded.

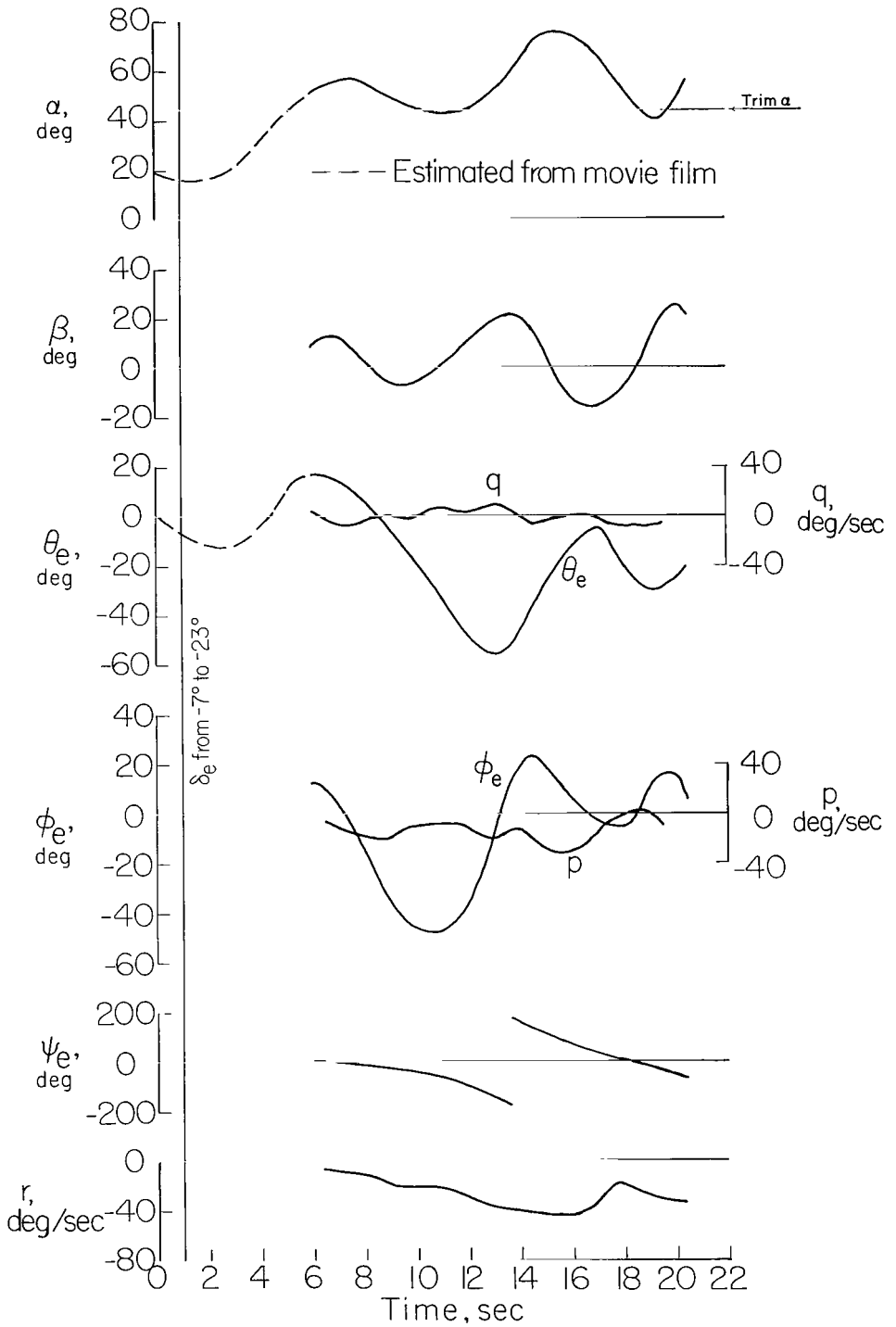

Figure 8.- Model motion with neutral ailerons; c.g. = 0.275c̄; launch condition: $\delta_e = -7^\circ$; $\delta_a = \delta_r = 0$.

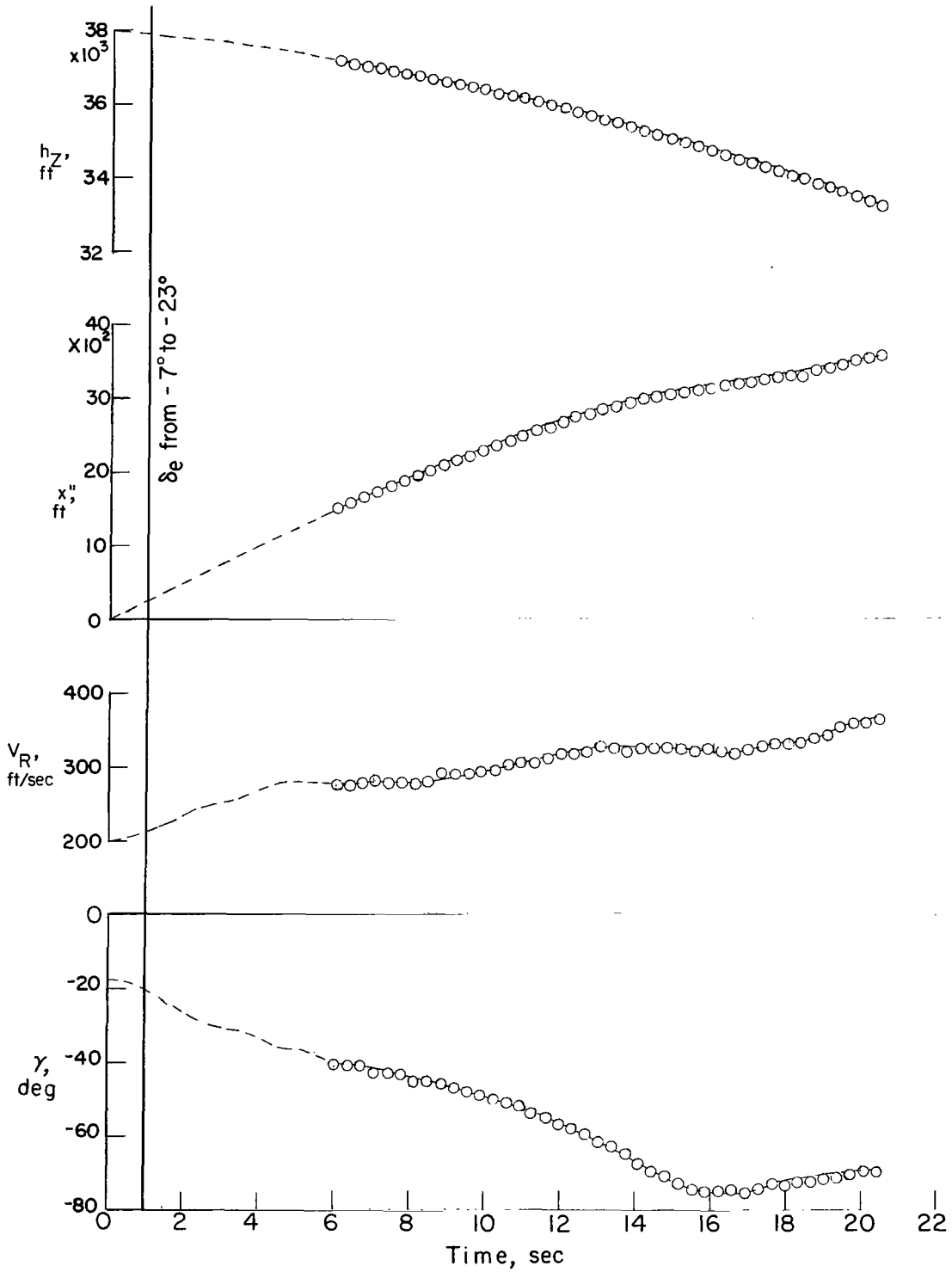

Figure 8.- Concluded.

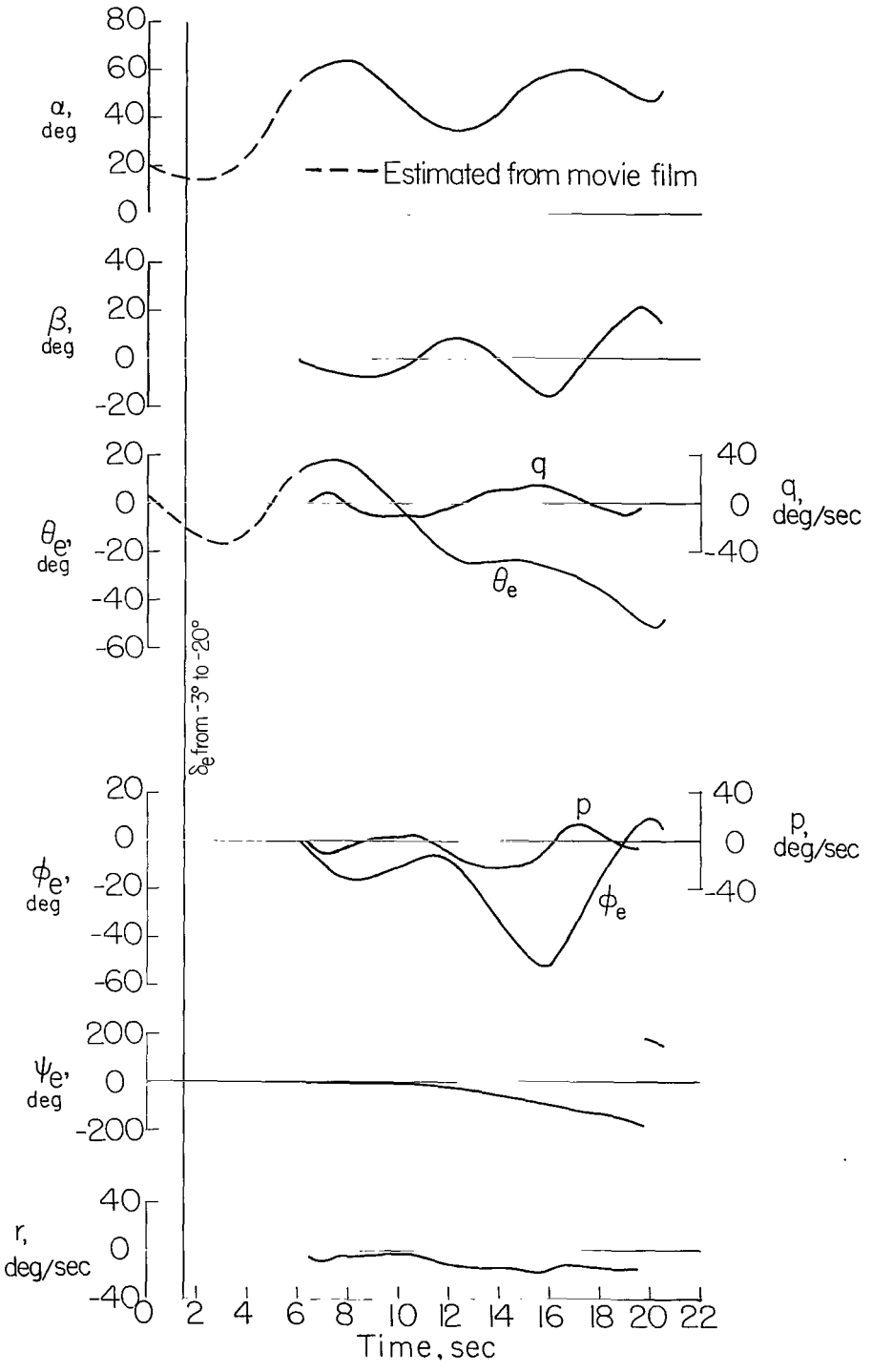

Figure 9.- Model motion with neutral ailerons; c.g. = 0.295$\bar{c}$; launch condition: $\delta_e = -3^\circ$; $\delta_a = \delta_r = 0$.

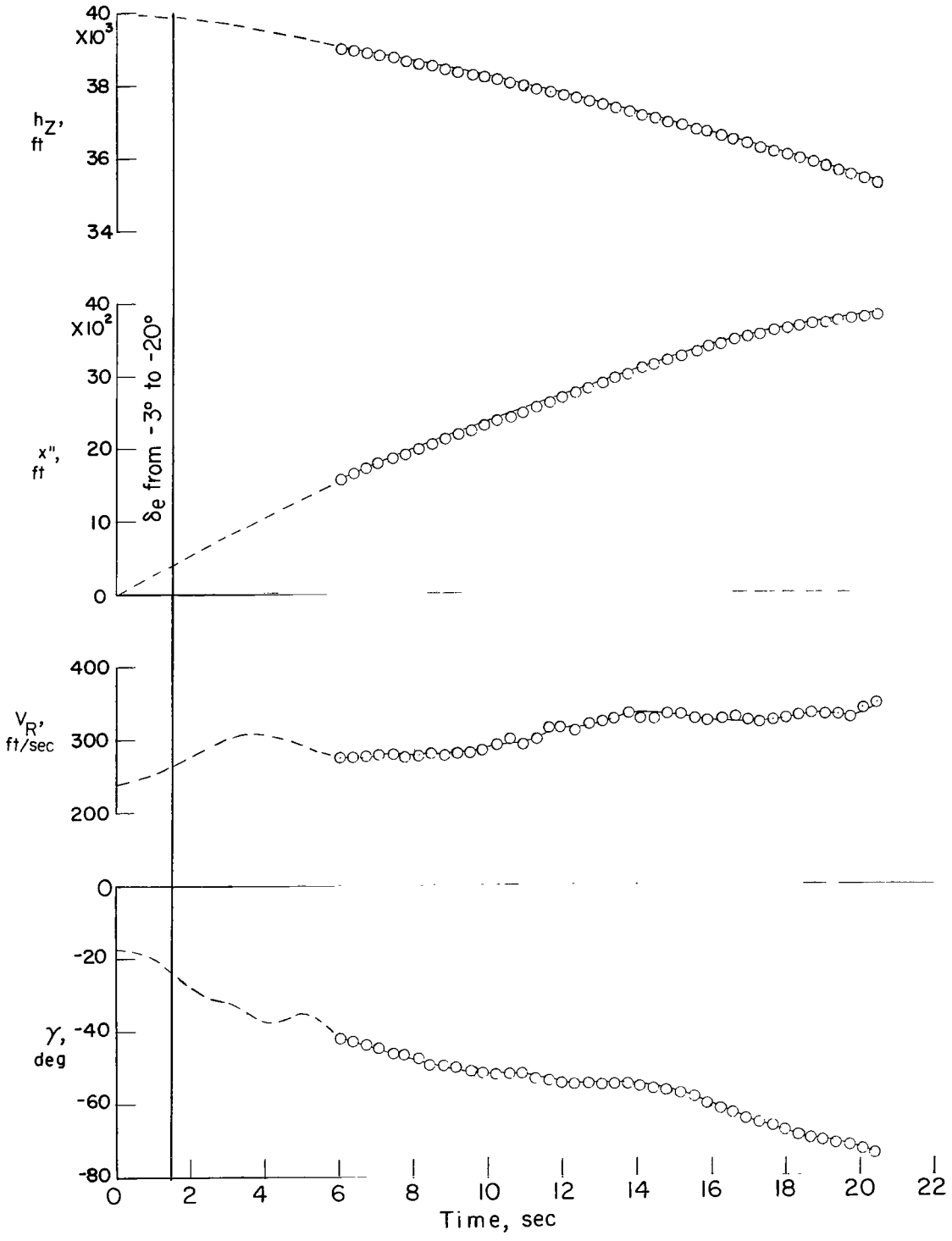

Figure 9.- Concluded.

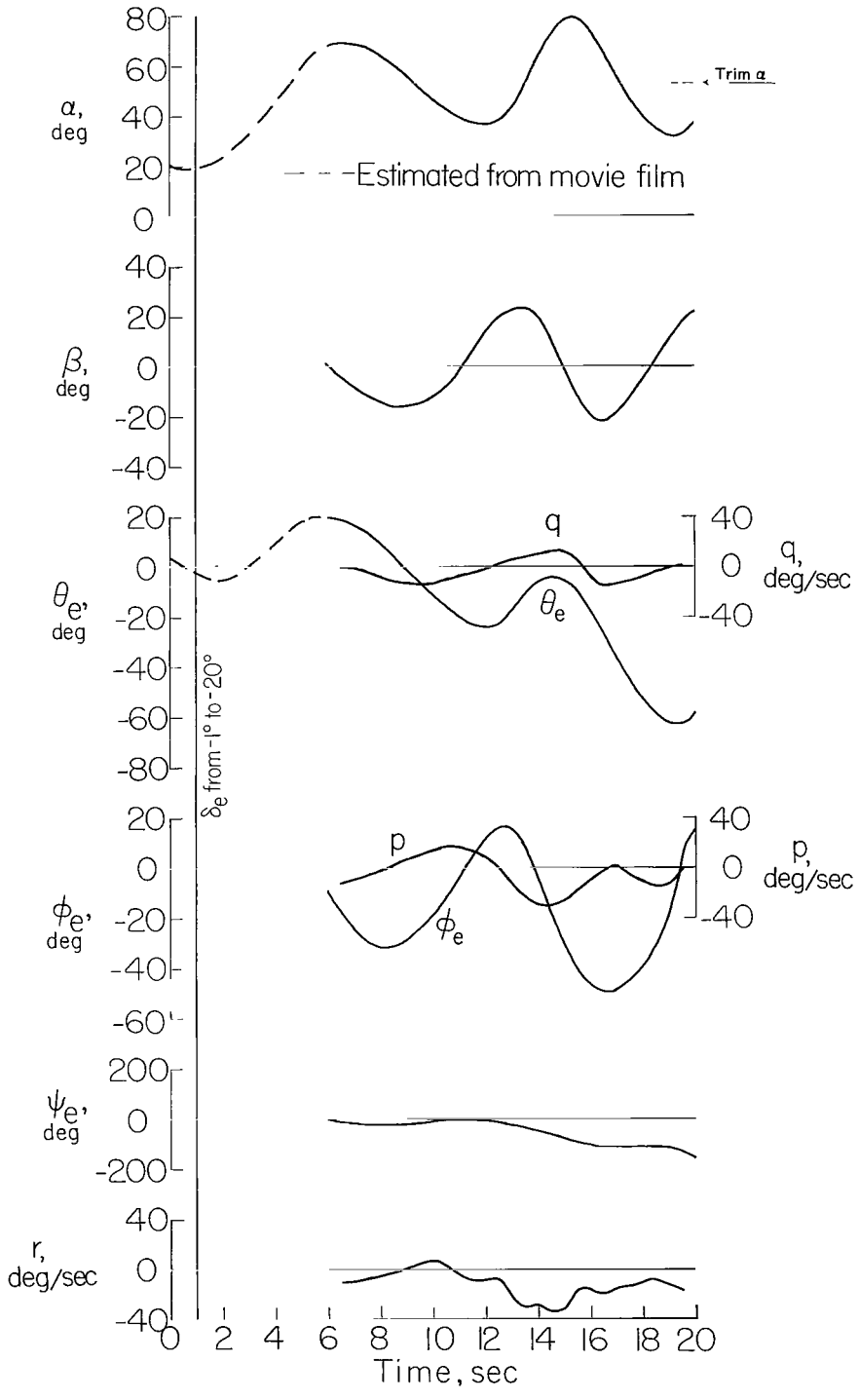

Figure 10.- Model motion with neutral ailerons; c.g. = 0.315$\bar{c}$; launch condition: $\delta_e = -1^o$; $\delta_a = \delta_r = 0$.

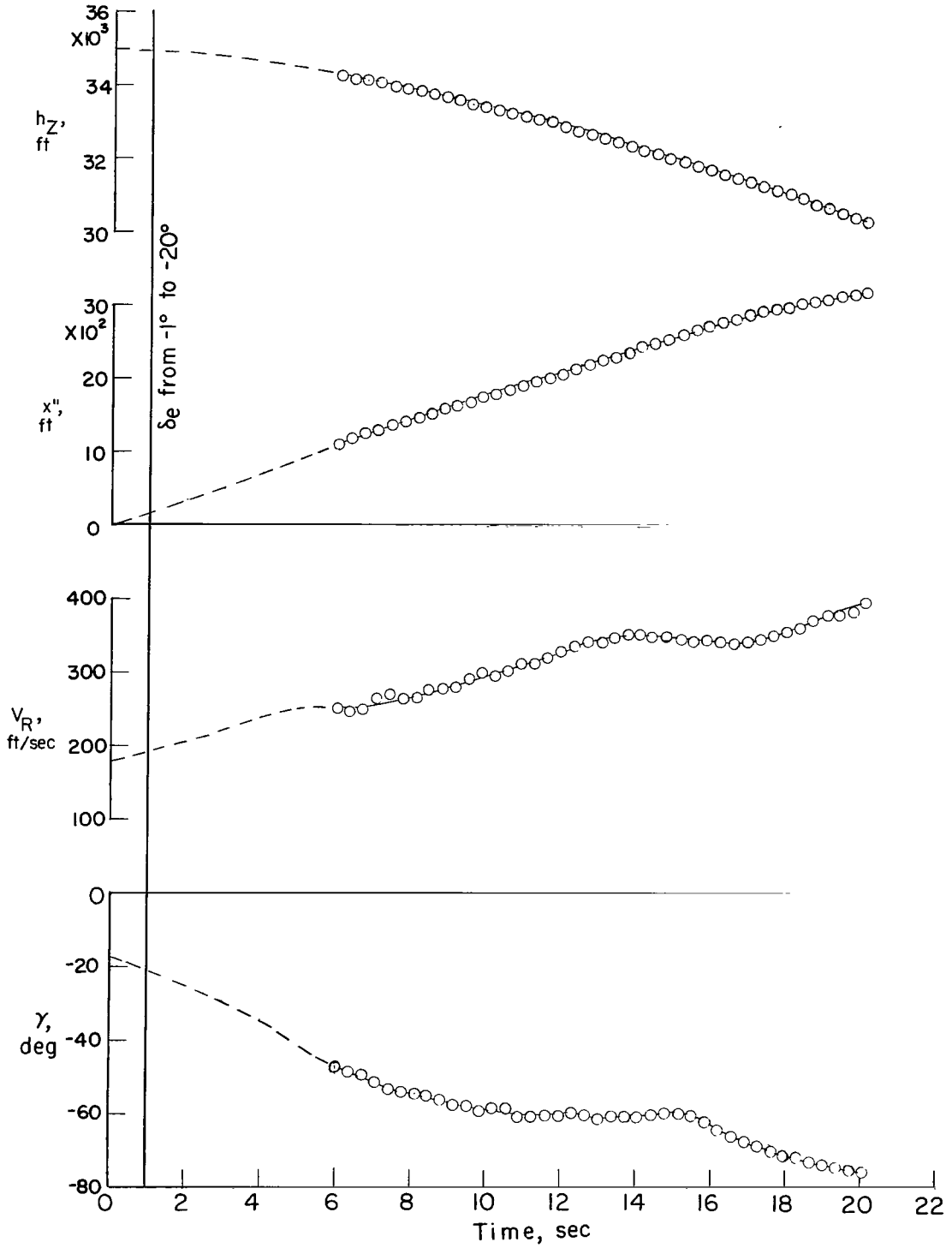

Figure 10.- Concluded.

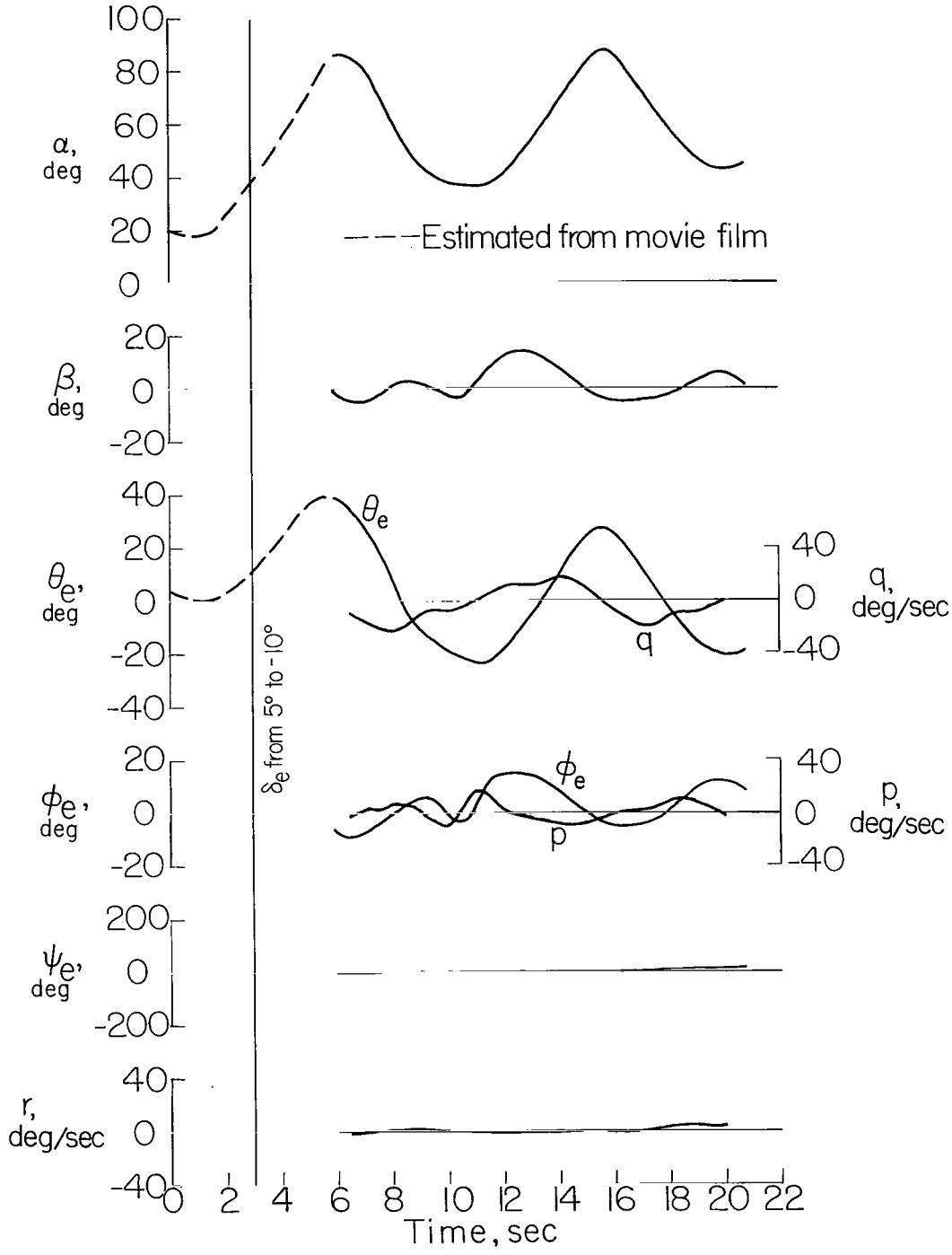

Figure 11.- Model motion with neutral ailerons; c.g. = 0.345$\bar{c}$; launch condition: $\delta_e = 5^\circ$; $\delta_a = \delta_r = 0$.

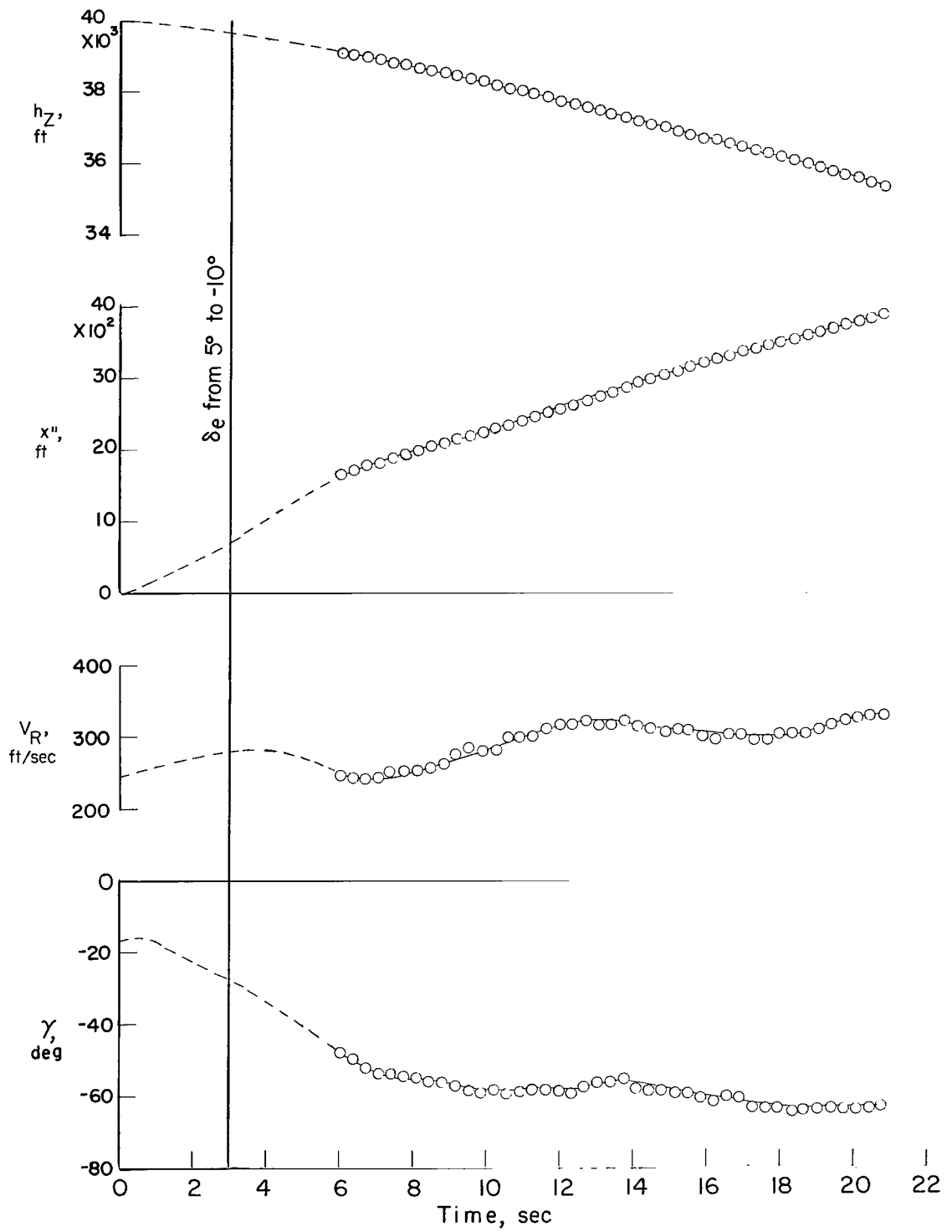

Figure 11.- Concluded.

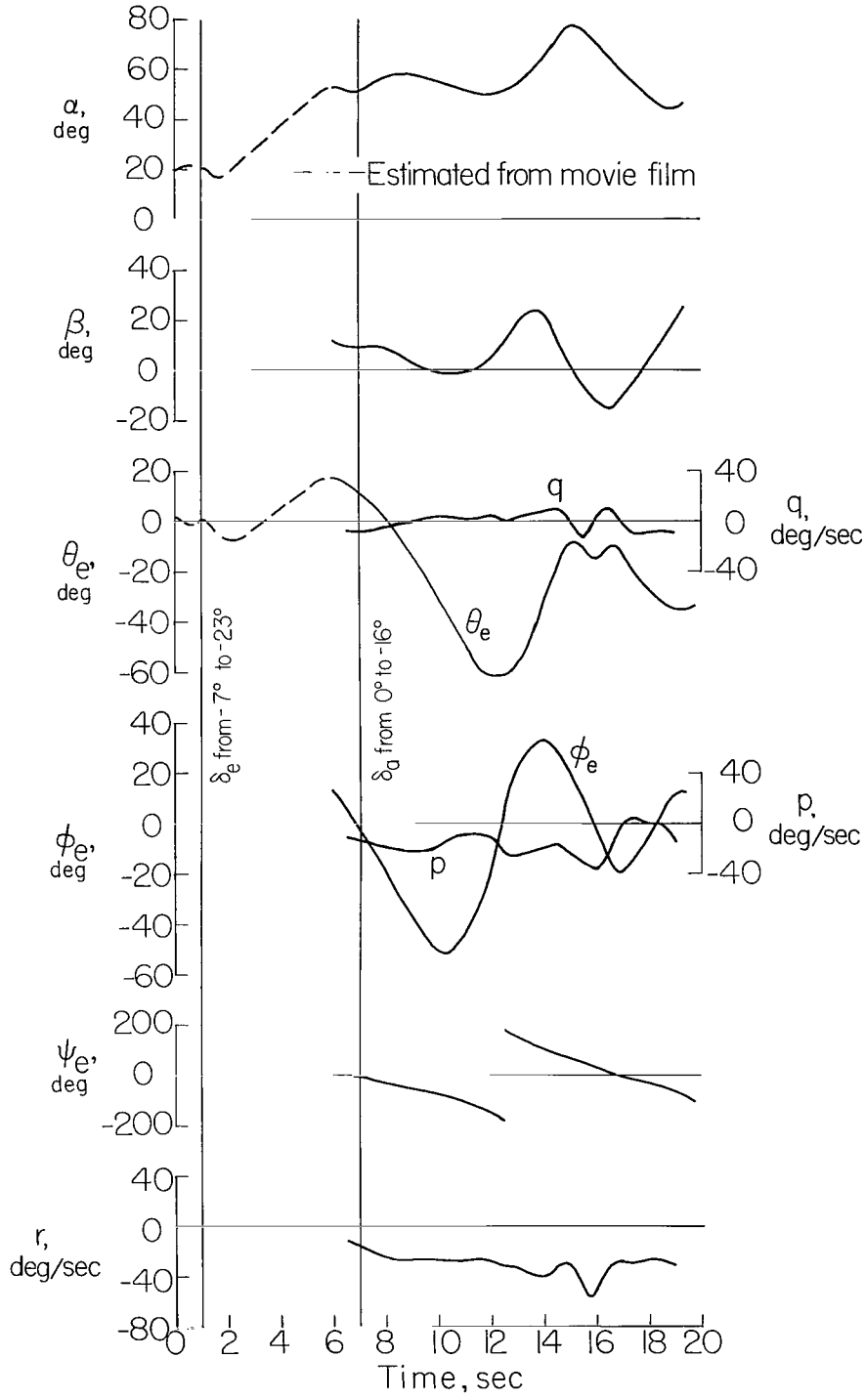

Figure 12.- Model motion with pro-spin aileron deflection; c.g. = 0.275$\bar{c}$; launch condition: $\delta_e = -7^\circ$; $\delta_a = \delta_r = 0$.

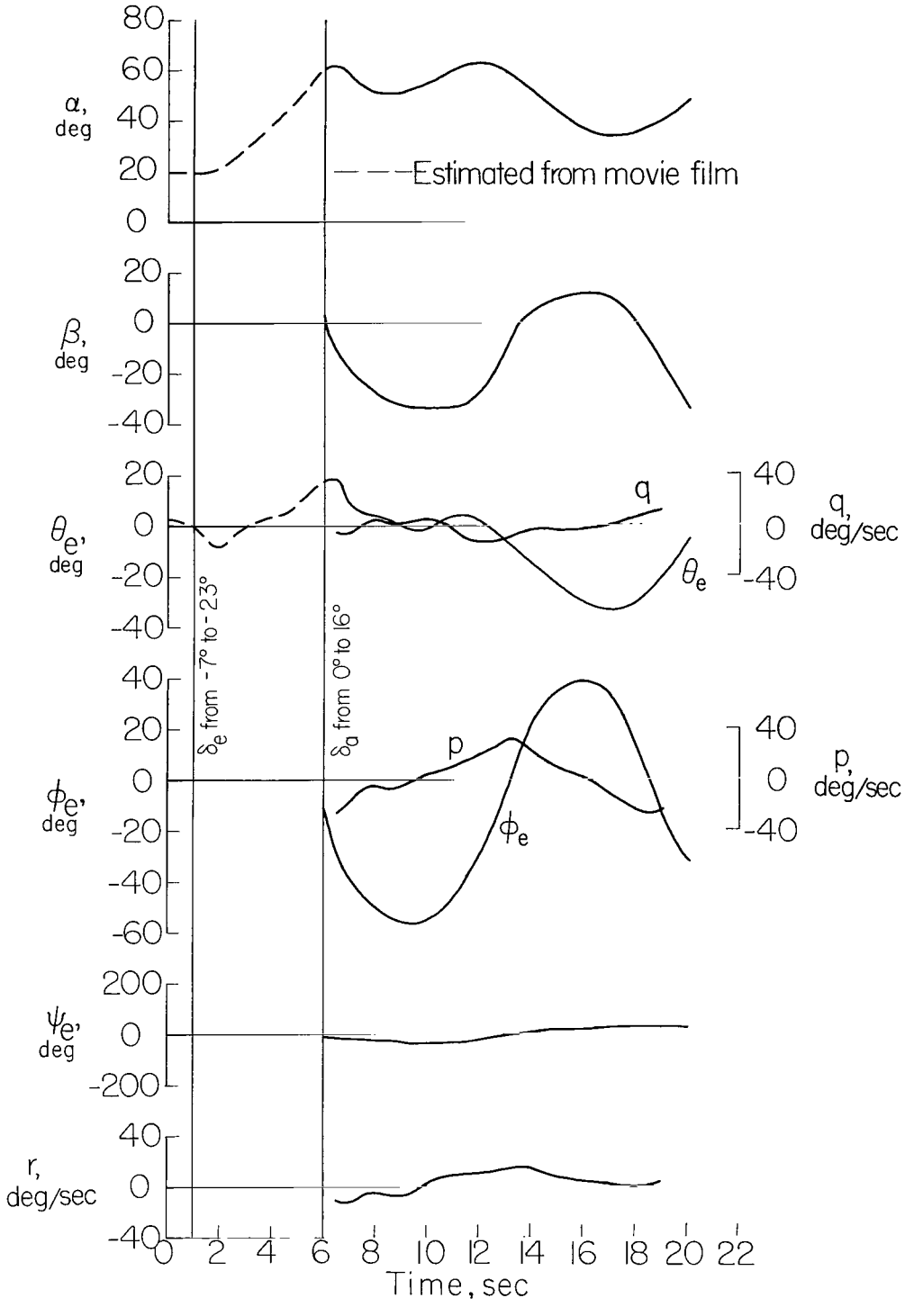

Figure 13.- Model motion with antispin aileron deflection; c.g. = 0.275$\bar{c}$; launch condition: $\delta_e = -7^\circ$; $\delta_a = \delta_r = 0$.

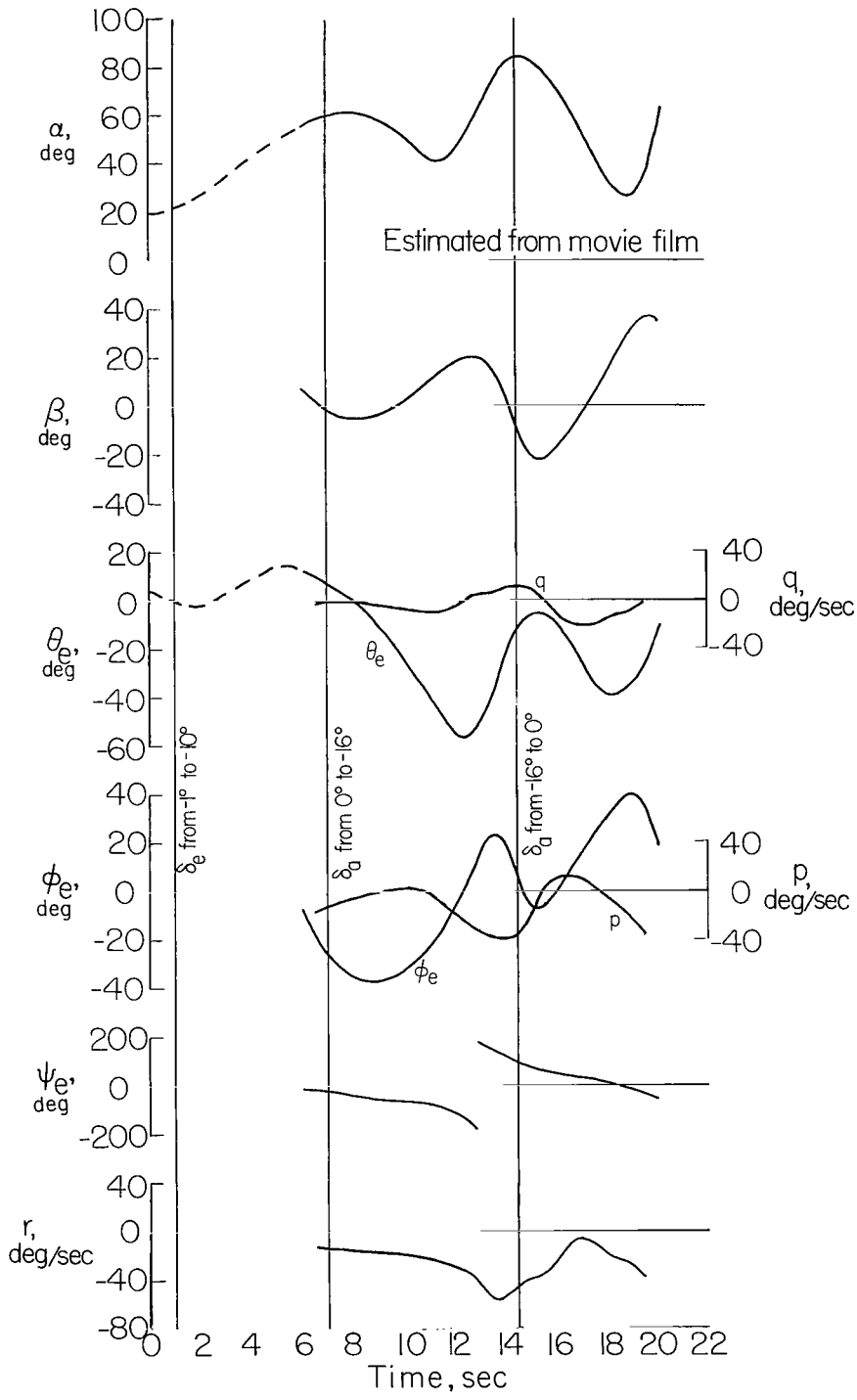

Figure 14.- Model motion with pro-spin aileron deflection; c.g. = 0.315$\bar{c}$; launch condition: $\delta_e = -1^\circ$; $\delta_a = \delta_r = 0$.

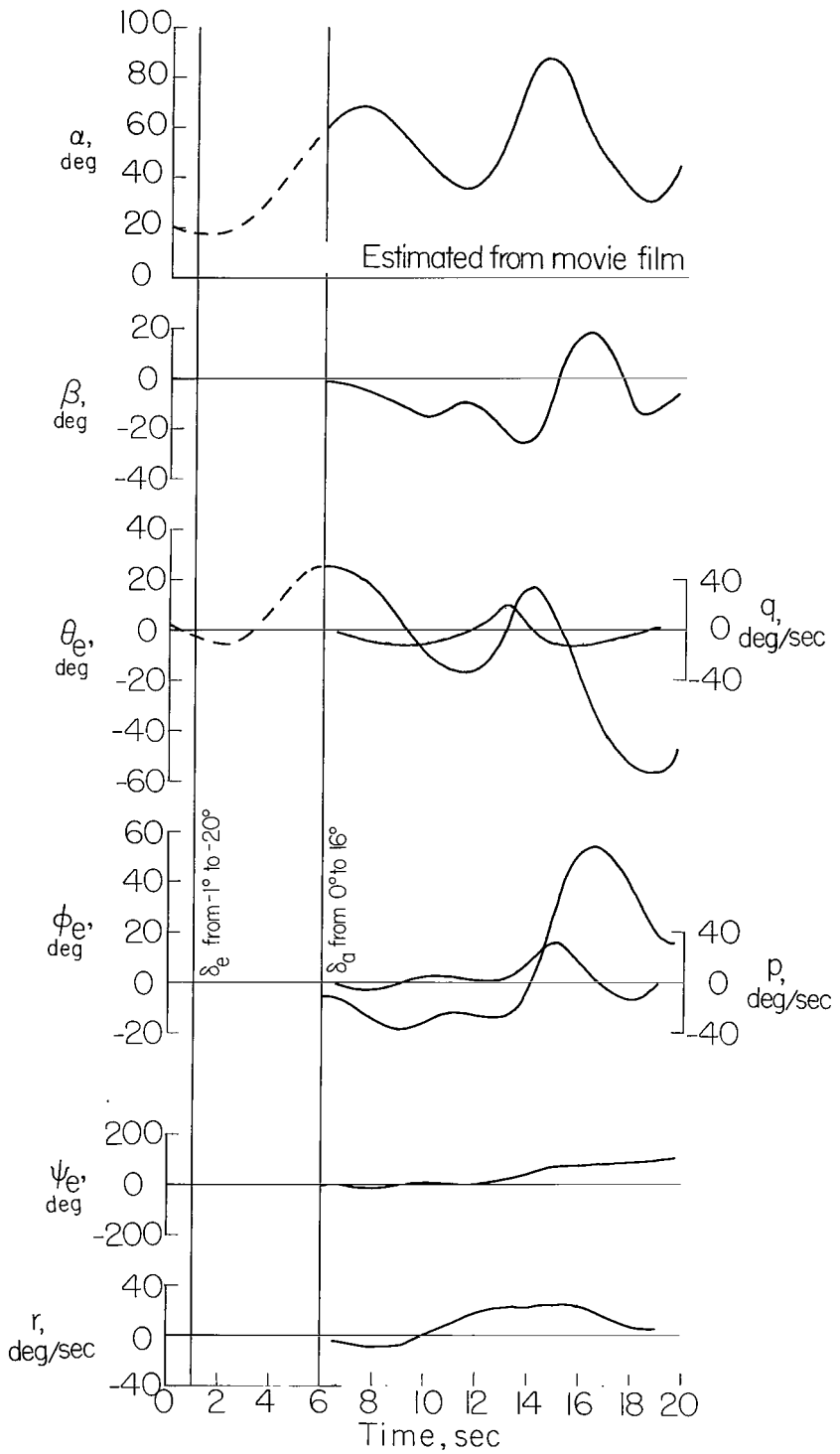

Figure 15.- Model motion with antispin aileron deflection; c.g. = 0.315$\bar{c}$; launch condition: $\delta_e = -1^\circ$; $\delta_a = \delta_r = 0$.

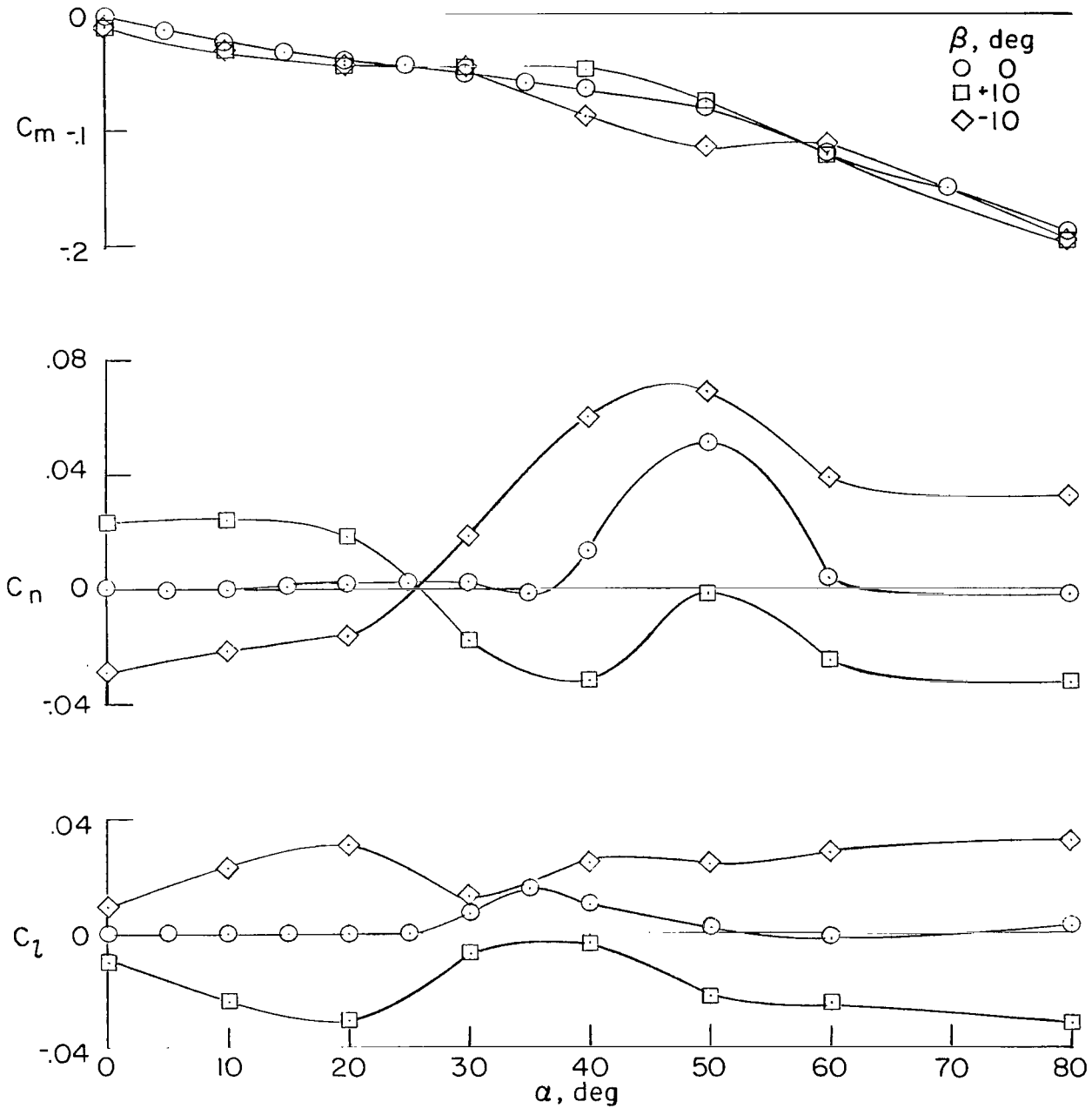

Figure 16.- Aerodynamic characteristics of a model for c.g. = 0.275$\bar{c}$; $\delta_e = \delta_a = \delta_r = 0$.

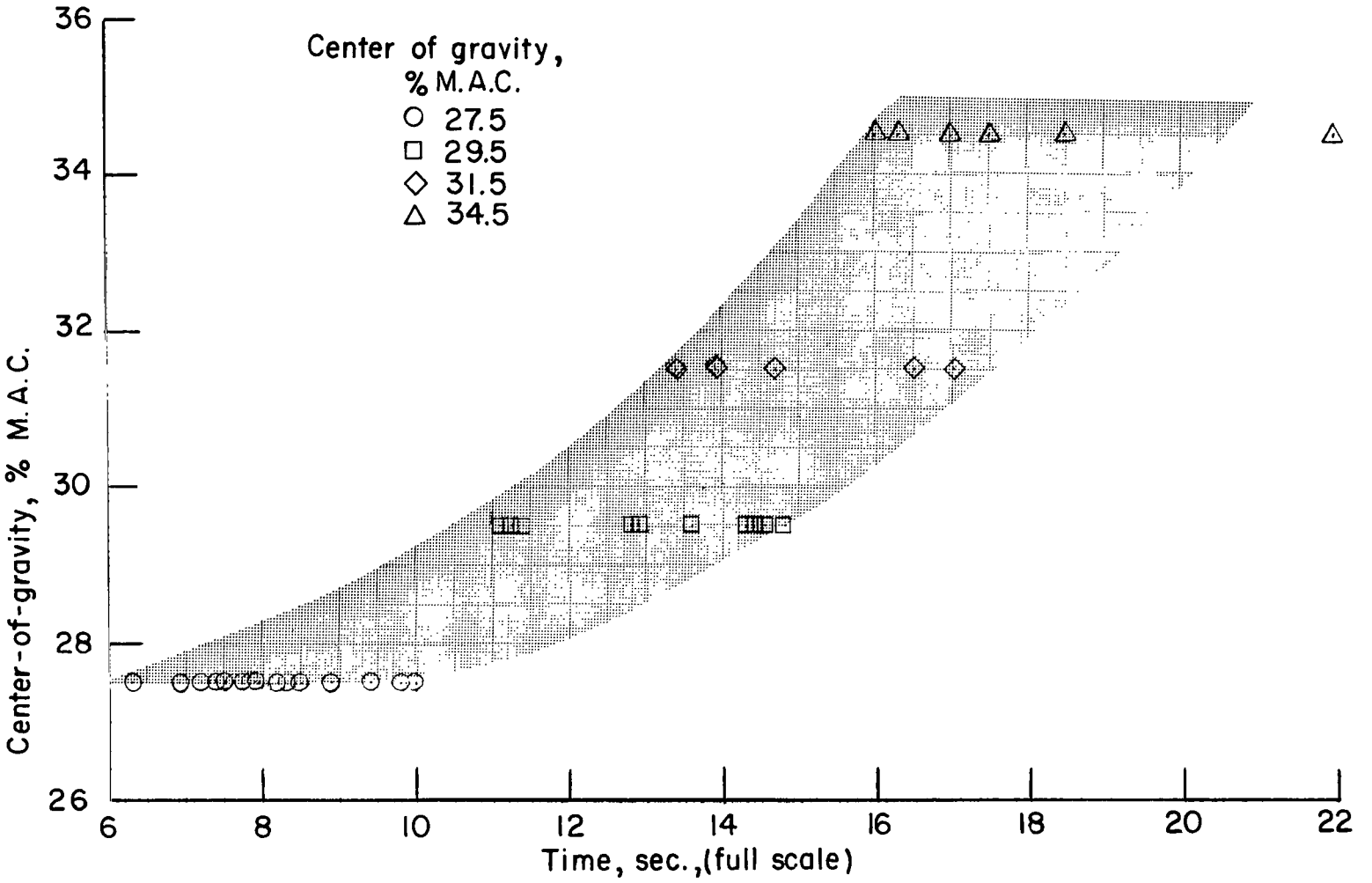

Figure 17.- Effect of center-of-gravity location on time required for model to yaw $\frac{1}{2}$-turn; $\delta_a = \delta_r = 0$.

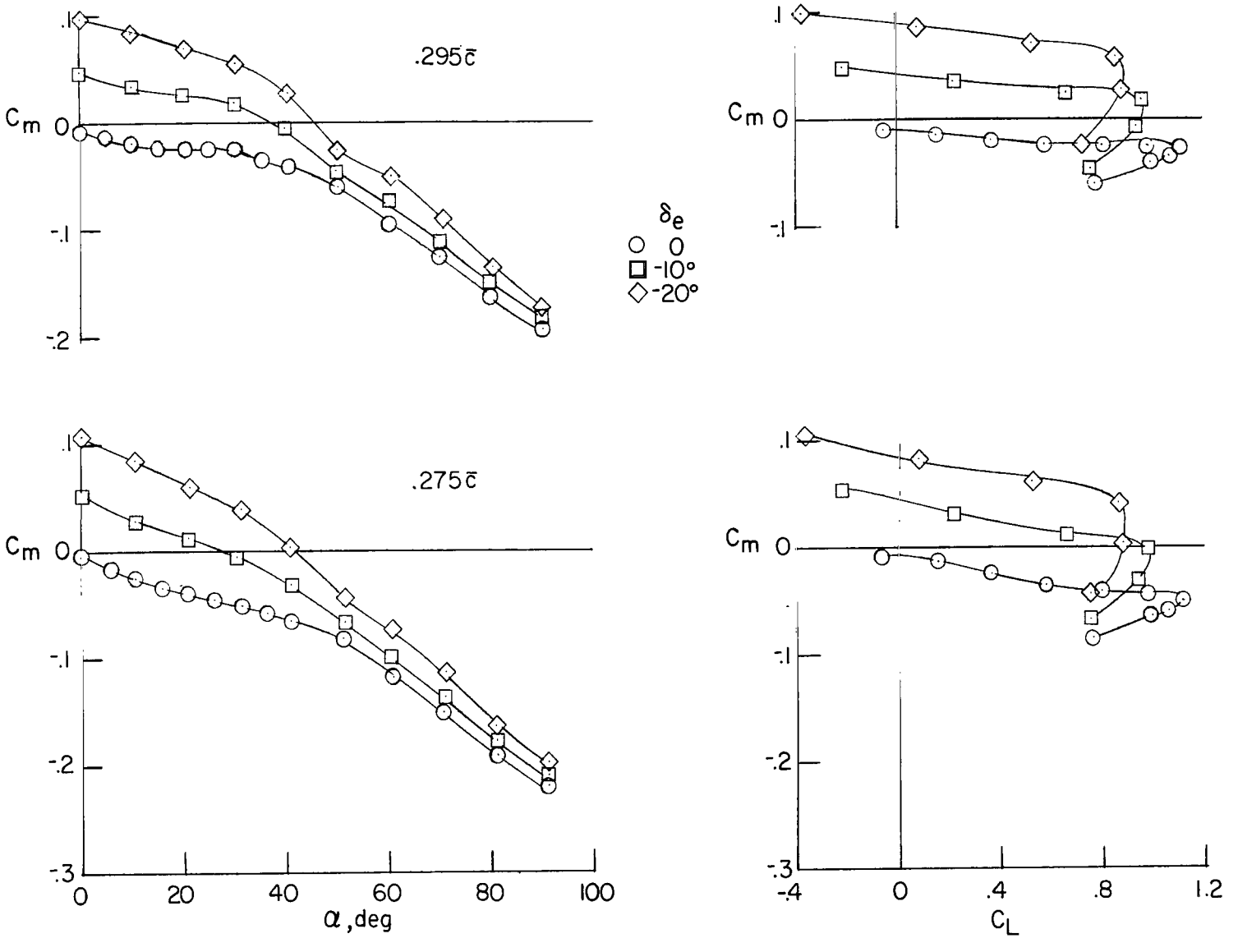

Figure 18.- Effect of center of gravity on the longitudinal stability characteristics of configuration.

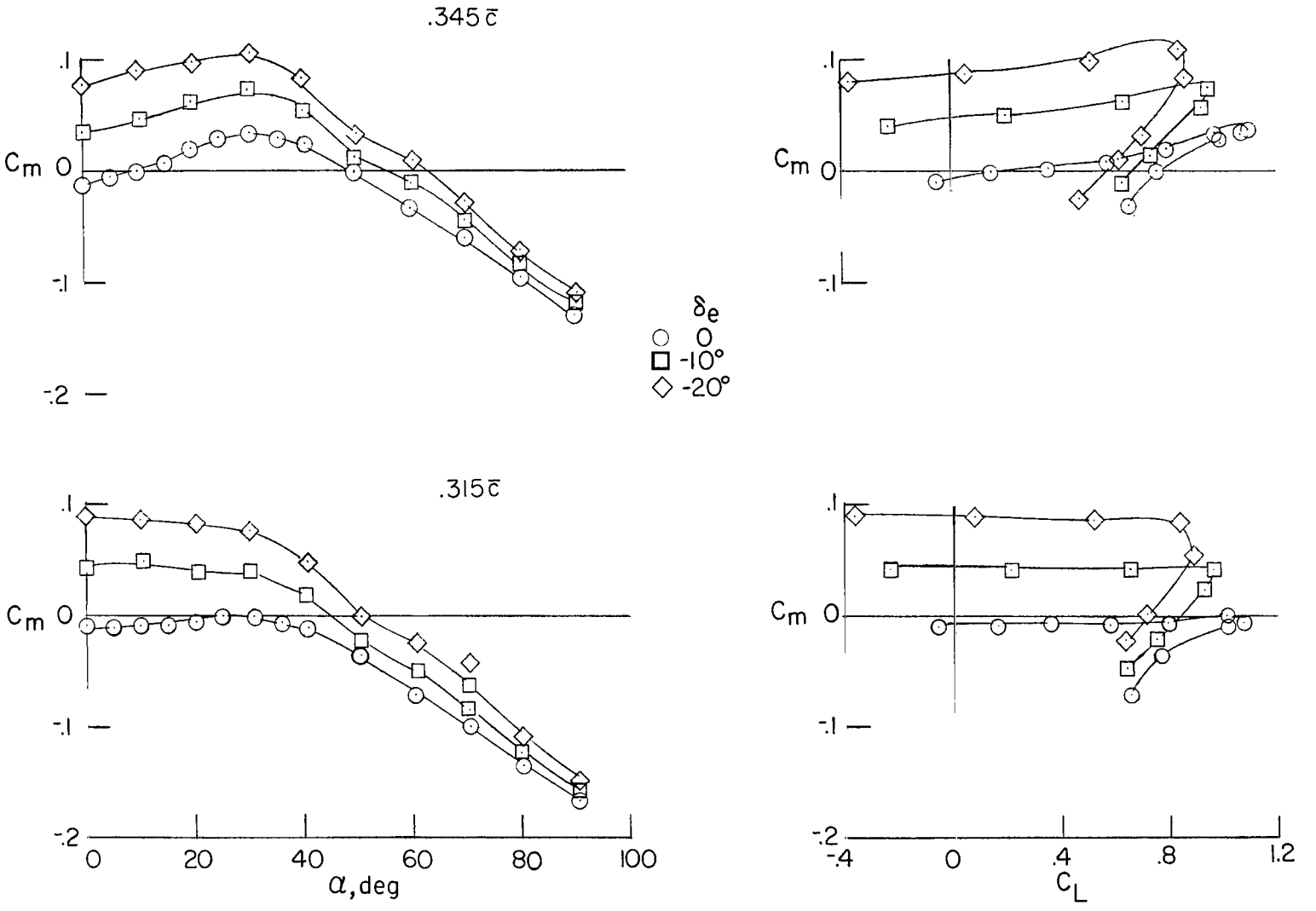

Figure 18.- Concluded.

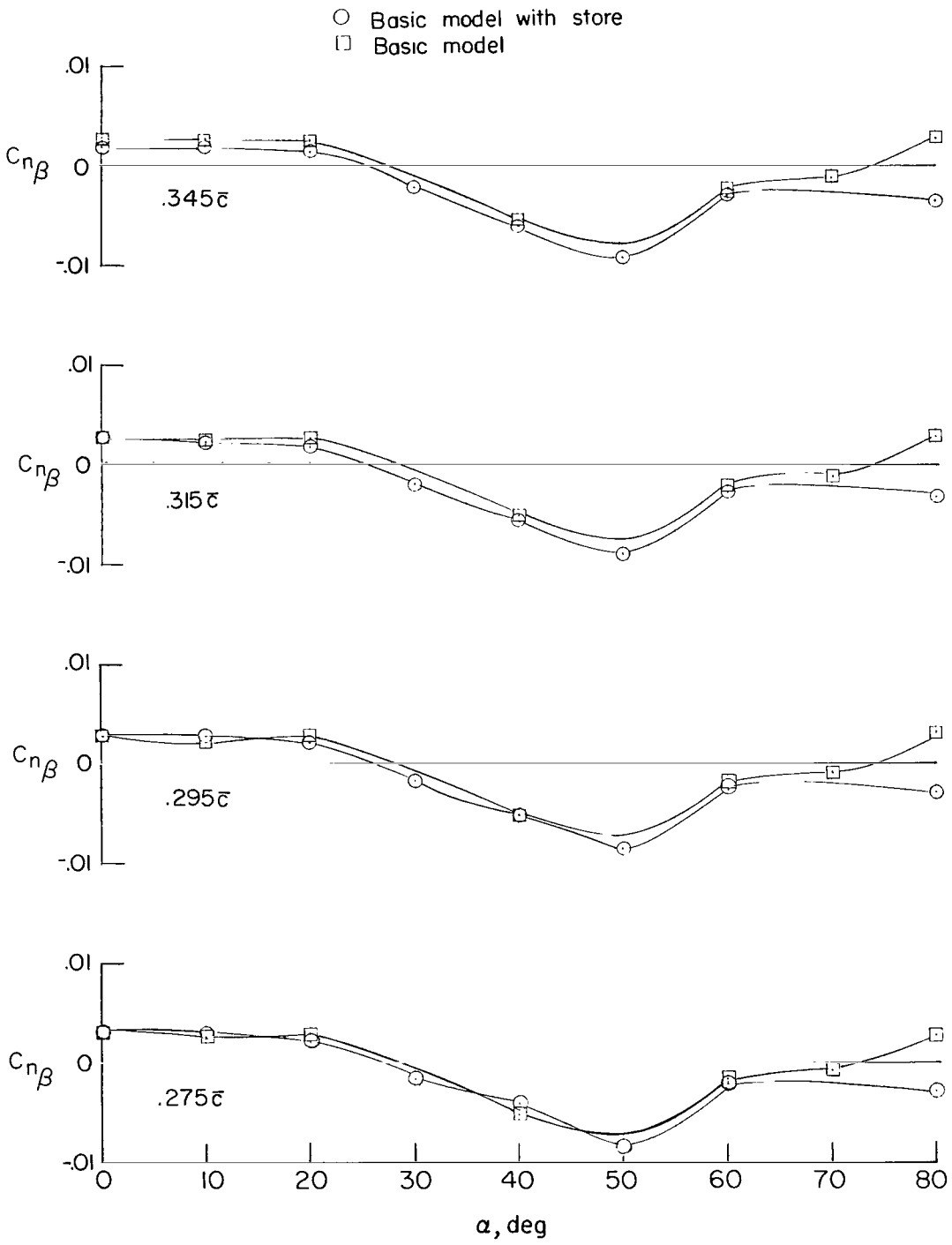

Figure 19.- Directional characteristics of model. $\delta_e = \delta_a = \delta_r = 0$. Derivatives are about the body axis.

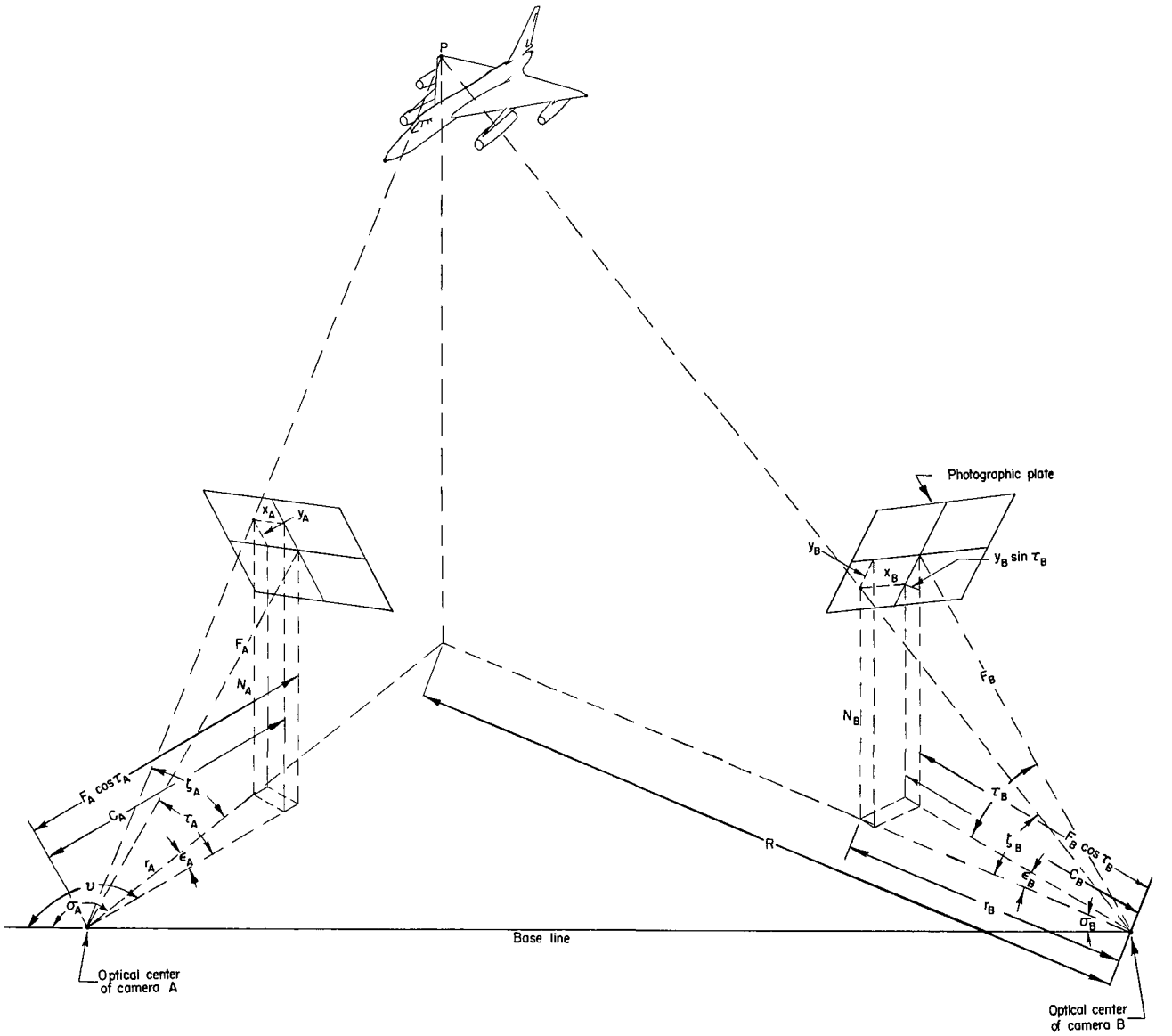

Figure 20.- Projection of reference point on model to show related angles between model, photographic plates, camera optical centers, and horizontal plane.

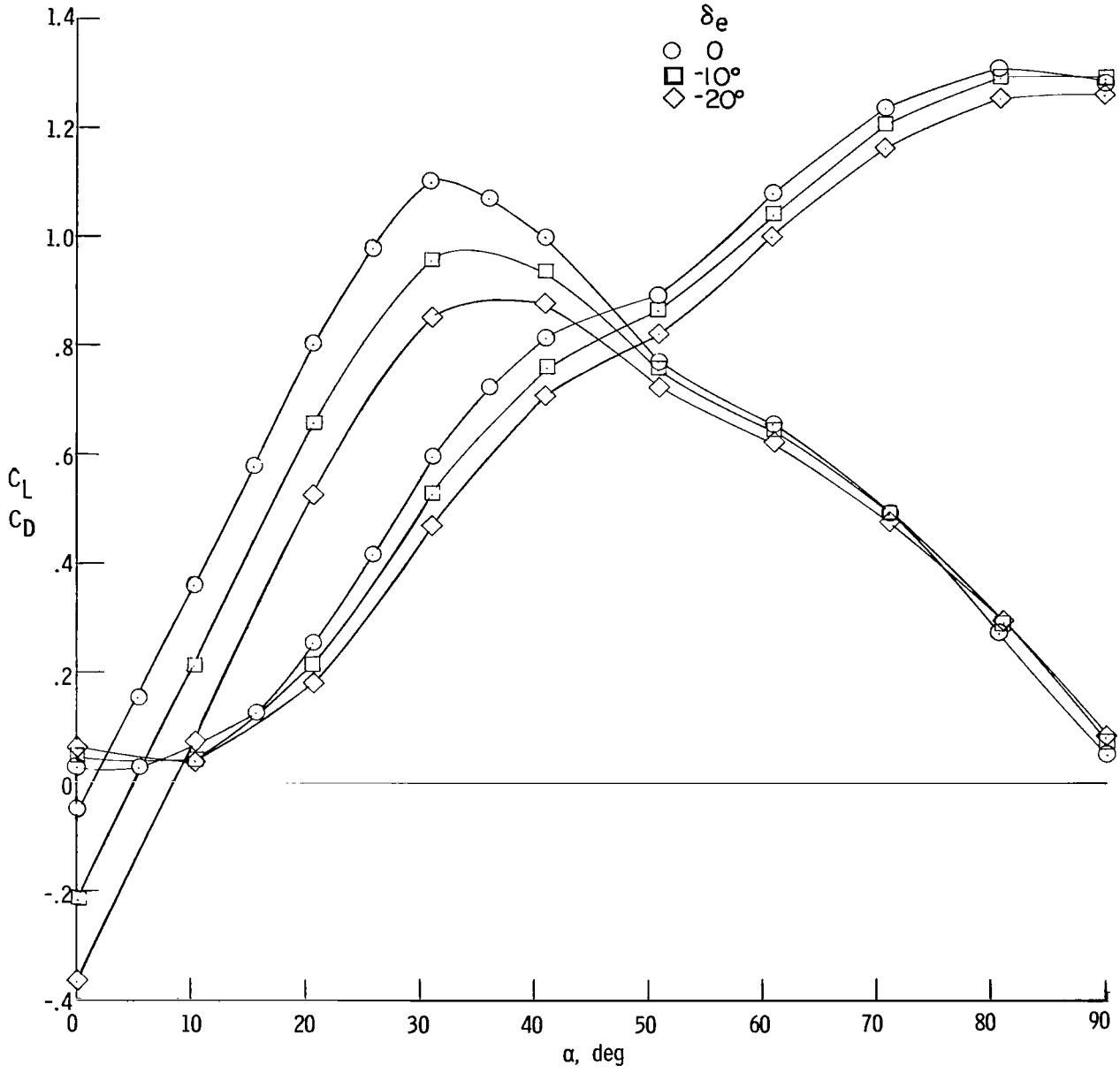

Figure 21.- Effect of elevator deflection on lift and drag characteristics of configuration up to 90° angle of attack.

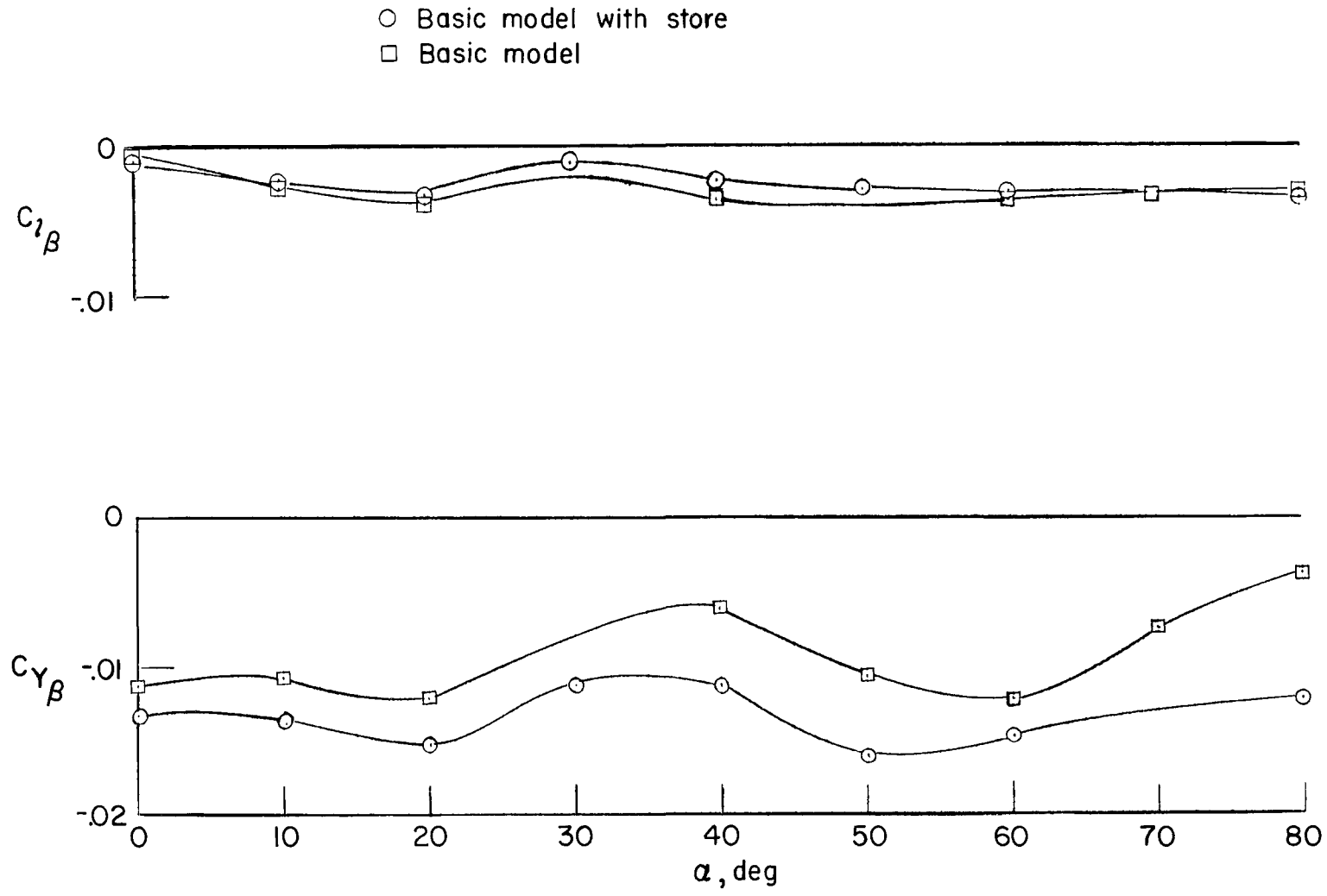

Figure 22.- Rolling-moment and side-force characteristics of model; $\delta_e = \delta_a = \delta_r = 0$; derivatives are about the body axes.

2/22/80

"The aeronautical and space activities of the United States shall be conducted so as to contribute . . . to the expansion of human knowledge of phenomena in the atmosphere and space. The Administration shall provide for the widest practicable and appropriate dissemination of information concerning its activities and the results thereof."

—NATIONAL AERONAUTICS AND SPACE ACT OF 1958

NASA SCIENTIFIC AND TECHNICAL PUBLICATIONS

TECHNICAL REPORTS: Scientific and technical information considered important, complete, and a lasting contribution to existing knowledge.

TECHNICAL NOTES: Information less broad in scope but nevertheless of importance as a contribution to existing knowledge.

TECHNICAL MEMORANDUMS: Information receiving limited distribution because of preliminary data, security classification, or other reasons.

CONTRACTOR REPORTS: Technical information generated in connection with a NASA contract or grant and released under NASA auspices.

TECHNICAL TRANSLATIONS: Information published in a foreign language considered to merit NASA distribution in English.

TECHNICAL REPRINTS: Information derived from NASA activities and initially published in the form of journal articles.

SPECIAL PUBLICATIONS: Information derived from or of value to NASA activities but not necessarily reporting the results of individual NASA-programmed scientific efforts. Publications include conference proceedings, monographs, data compilations, handbooks, sourcebooks, and special bibliographies.

Details on the availability of these publications may be obtained from:

SCIENTIFIC AND TECHNICAL INFORMATION DIVISION

NATIONAL AERONAUTICS AND SPACE ADMINISTRATION

Washington, D.C. 20546